SIMULATING DUNE GROWTH AT A MEGA NOURISHMENT

MSC THESIS

A.F. DE BRUIN

2023

TU Delft

Simulating dune growth at a Mega Nourishment

By

Aaron de Bruin

in partial fulfilment of the requirements for the degree of

Master of Science

in Civil Engineering

at the Delft University of Technology,

to be defended publicly on

Student number: 4394658

Supervisors: Dr. Ir. A. P. Luijendijk
Msc. T.T. Kettler
Ir. B van Westen

Thesis committee:

Dr. Ir. M.A. de Schipper
Dr. ing. M.Z. Voorendt

Summary

Currently, almost a quarter of the sandy coasts around the globe are eroding and this number is likely to grow due to sea level rise. To counter this coastal erosion and the inherent hazards, nourishments are carried out. Since sea level rise rates are increasing, nourishment volumes should increase as well. This led to the pilot Mega-Nourishment project the Sand Motor. However, measurements showed significantly lower dune growth rates than predicted. To use Mega-Nourishments as flood protection in the future, a better understanding of the aeolian sediment transport processes is necessary. This study focussed on identifying and implementing of these processes into a process-based aeolian transport model, after which the model was validated.

For this study the model AeoLis was chosen. First, the AeoLis software was tested and improved based on the identified processes. After verification, a case study was chosen and implemented in the program. Then a model evaluation was carried out to assess AeoLis' performance. This evaluation was based on detailed measurements of the Delfland coast taken during the first ten years of the Sand Motor. Due to the large variation in coastal profile at the Sand Motor, not only integrated dune growth volumes are evaluated but alongshore variation in dune growth as well. After the model evaluation, the impact of different water levels and coastal profiles was assessed.

On integrated scale, the outcome of this study showed that during the first years, the dune growth computed by AeoLis is almost identical to the measured dune growth, both at the regular Delfland beach and in the proximity of the Sand Motor. However, later on in the simulation the deviations between computed and measured growth increase due to the absence of marine processes in the model and the subsequent differences in morphology between model and reality.

The alongshore variation in dune growth showed promising results as well. However, in reality, disturbances in the alongshore dune growth are partly due to presence of walkways and beach clubs. In the model there are no walkways and beach clubs present. The disturbances in the modelled alongshore dune growth are due to shadow effects, caused by the dune foot definition. Despite those differences, the underlying alongshore dune growth trend is captured well.

The study leads to the conclusion that process-based aeolian transport modelling is capable of accurately simulating alongshore dune growth at Mega-Nourishments. However, due to lack of marine processes in the model and the subsequent bathymetry differences between model and reality, the accuracy decreases over simulated time. Therefore, a coupled hydrodynamic-aeolian model would be the next step in improving the long-term predictability of dune growth at Mega-Nourishments.

Acknowledgements

This MSc thesis report is the completion of my master's degree in Hydraulic engineering. I would like to express my gratitude to both the Delft University of Technology and Deltares for facilitating the completion of this thesis. Especially thanks to the members of my thesis committee, for the great support and help during the many meetings we had; Arjen, Tosca and Bart for helping and sharing the expert knowledge, Matthieu as chair of the committee and Mark for the finishing touch.

I am proud to be part of the ongoing research about aeolian processes and modelling. This concludes the time at the TU Delft for me as a student.

And now for something completely different.

Aaron de Bruin
Delft, June 2023

Contents

1 Introduction

1.1 Motivation for the present research

Currently, 24% of the world's sandy beaches, including the majority of the sandy shorelines in marine protected areas, are eroding at a rate of more than 0.5 m/year [9]. Due to sea level rise, this rate is expected to increase. Erosion of sediment in these coastal zones can result in the landward migration of the shoreline [31]. Retreating shorelines not only impact environmental and ecological aspects of the coast but can also be a major concern for the population, with twenty-one of the thirty-three world's largest cities located within the coastal area [25]. To ensure sufficient flood protection for the hinterland, an improvement of the knowledge about dune growth and aeolian transport is necessary. Process-based modelling could improve this knowledge and the predictability of dune development. For this, further research is required.

1.2 Sea level rise

New studies show that the mean sea water level is likely to increases much faster than previously anticipated. Sea level rise has great influence on the morphological development of sandy coasts. The Intergovernmental Panel on Climate Change (IPCC) predicts that sea level rise will accelerate for the coming decades or even centuries [6]. A rise in sea levels induces erosion of the coastal profile. Landward recession of the shorelines in already densely populated areas would result in so called 'coastal squeeze'; a process where the retreat path of the shoreline is blocked by inhabited coastal areas. To prevent 'coastal squeeze', measures must be taken.

The intergovernmental Panel on Climate Change (IPCC) is the United Nations body for assessing the science related to climate change. The purpose of the IPCC is to provide policymakers with scientific assessments on climate change. In the latest report IPCC AR6, which came out in 2021, it is stated that future SLR is highly dependent on climate policy. The panel came up with five different scenarios. These Shared Socioeconomic Pathways (SSP) scenarios are made to describe the development of greenhouse gasses as a consequence of five different climate policies. These scenarios are named as SSPx-y where the x stands for the socio-economic pathway, ranging from one to five. The y stands for the approximate level of radiative forcing [W/m^2], resulting from the pathway, in the year 2100. Lower future GHG emissions result in lower x and y values and vice versa.

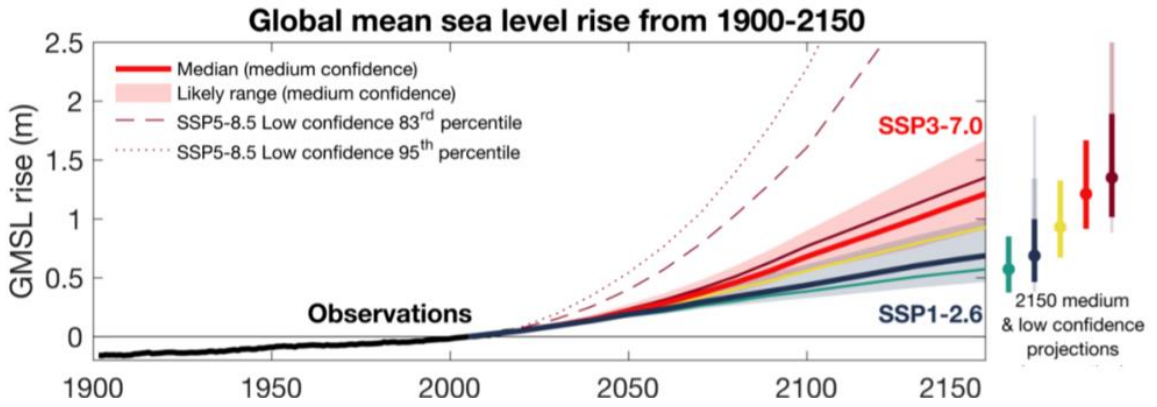

Figure 1 GMSL change from 1900-2150 projected under the SSPx,y scenarios. Solid lines show median projections. The bars at the right show likely ranges including 17th-83rd/5th-95th percentile ranges for SSP1-1.9 and SSP5-8.5. Shaded regions show likely ranges from SSP3-7.0 and SSP1-2.6. [6]

To protect the Netherlands from the climate change and rising sea level, the Dutch government came up with the Delta program. This program contains rules, decisions and strategies to ensure safety and are based on the Royal Dutch Meteorological Institute (KNMI)'14 scenarios. The

calculations of these scenarios are in turn based on the IPCC AR5 report which came out in 2014. The scenarios considered a maximum SLR value of 0.4m in 2050 and 1.0m in 2100. Recent reports, including the IPCC AR6, show more extreme SLR predictions. The KNMI will present an updated version of the KNMI'14 in 2023. This version will include the findings of the IPCC AR6 report and can be used to adjust current Delta program strategies. In October 2021 the KNMI already published Klimaatsignaal'21, which is a report based on the IPCC AR6 that can be used until the final KNMI'23 report comes out. The SLR at the Dutch coast, predicted by the KNMI's Klimaatsignaal'21 is shown below (Fig 2).

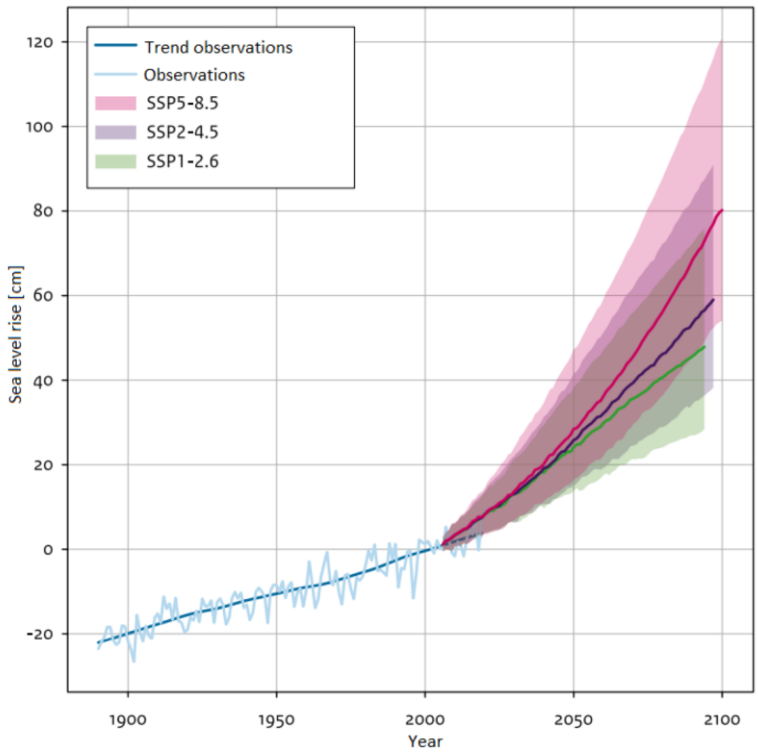

Figure 2 SLR at the Dutch coast. Observed and according to the new SLR scenarios. Solid lines show median projections and the shaded regions show the 90% bandwidth. [7]

1.3 Coastal erosion

Due to the rising sea levels, the sediment demand of a coastal stretch will increase as well. Where those demands are not met, erosion takes place. Along most sandy coasts, accelerated SLR is likely to result in the permanent inundation of unprotected low-lying land and more frequent episodic coastal inundation where wave conditions and storm surge act in combination with SLR [8]. SLR causes larger water depths in front of coasts. Therefore, there will be less bottom friction and wave breaking in the surf zone, resulting in less wave energy dissipation and larger wave attack. The wave attack takes places higher up in the coastal profile as well, impacting dunes further land inward.

To assess the effects of SLR on a sandy coast the Bruun rule can be applied. This is the most common method to determine the coastline retreat as a consequence of SLR and is based on a two-dimensional mass conservation principle where a translation of the beach and bottom profile results in shore recession and deposition of sediments [10].

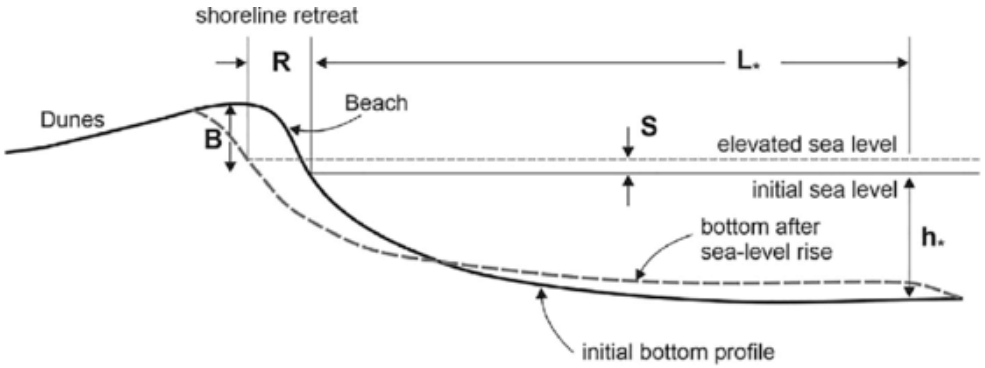

Figure 3 Geometric response of the coast to sea level rise [11].

The shoreline retreat can be calculated as a function of the coastal profile and the SLR. The model suggests that shoreline recession is in the range 50 to 200 times the rise in relative sea level [9]. Although the model offers a quick insight in the response of a sandy coast to a certain rise in sea level, it has several shortcomings. One of the disadvantages of the Bruun Rule is that it does not account for gradient in longshore transport, where gradient in longshore transport can be a major factor in sediment erosion and deposition in coastal regions. Other points of criticism are the absence of time needed to reach a new equilibrium profile and its mass conservation assumption. Multiple papers have been published criticizing the Bruun Rule [13] and stating that no study has produced comprehensive verification of the rule [14]. However, the alternatives to this rule are often complex and not user-friendly. Therefore, the Bruun Rule is still used to determine the amount of shoreline recession as a consequence of SLR.

1.4 Dutch coastal management

With more than half of the inhabitants living in areas prone to flooding, The Netherlands are in constant war against water [33]. The primary defence against flooding are the dunes. Dunes are dynamic landforms composed of wind- and water-driven sand. When a coast experiences erosion or accretion of sediment, the shoreline tends to move landward or seaward respectively. The Dutch coast is experiencing erosion for centuries and the yearly retreat of the shoreline during the past 200 years is estimated to be between 0.5 and 1.5 metres per year [15]. A landward moving shoreline not only impacts the environment and ecology but has large negative impact on the population living in coastal areas as well [32]. To counter coastal erosion, sand nourishments can be applied. To prevent the shoreline from retreating even further, nourishments are carried out. The yearly total volume of nourishments along the Dutch coast is currently around 12 million m^3[2]. Due to sea level rise this volume is expected to grow even larger.

In the period of 1950-1970 most nourishments applied to the Dutch coast were small scale nourishments and were applied to counter the erosion due to storm events. Around 1970 the first large-scale nourishments were applied to compensate the erosion of sediment in the coastal cell. [36]. The average yearly nourished volume between 1970 and 1990 is around 3.5 M m^3 (Fig 4). In 1990, the Dutch government came up with the Kustnota 1990 in which the strategy to ensure coastal safety is described. It states that the future coastline should be maintained at the position as it was in 1990.

At the same time the building with nature concept became more important which holds that hard measures like revetments and groynes should only be applied when more nature friendly alternatives wouldn't suffice. Therefore, the preferred method to ensure a stable coastline is by increasing the nourishment volume. In the first years of maintaining the shoreline position, most nourishments were applied to the beach. However, it's generally cheaper to apply a nourishment on the shoreface than on the beach. Shoreface nourishments are approximately as effective as beach nourishments, in terms of maintaining the coastline position. Consequently, shoreface nourishments are often more cost-effective than beach nourishments [37]. Shoreface nourishments can positively affect the coastal state by acting as a (reef) berm for incoming waves as well [34]. All in all, shoreface nourishments became the more popular alternative and were applied more often over the years. Another thing to note is that from the year 2000 the nourishment volumes increase where the number of nourishments remain around 10 per year (Fig 4). This indicates that nourishments become larger in volume instead of an increase in nourishment frequency.

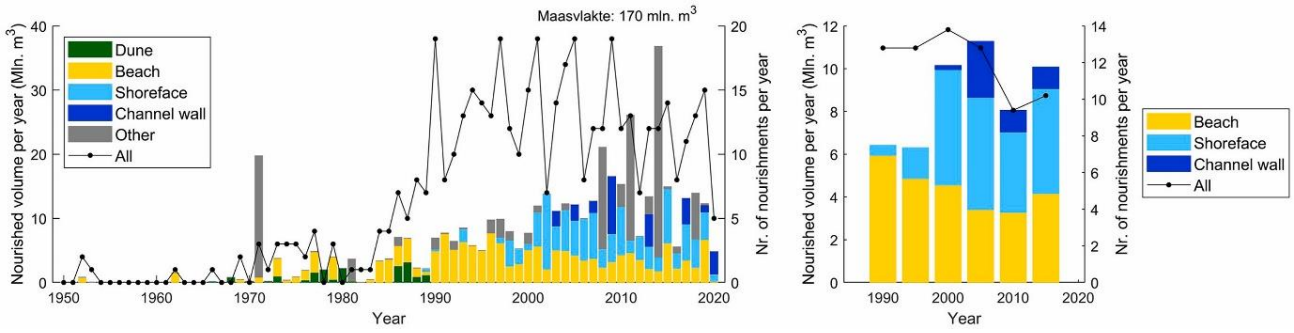

Figure 4 Annually nourished volume (bars, in million m3) per type of nourishment and the number of nourishments (line). Left: all sand nourishments, visualized per year. Right: nourishments within the dynamic conservation policy per period of 5 years [35].

From an ecological and recreational point of view, larger nourishments are preferred above an increase in frequency [26]. This led to the construction of a so-called mega-nourishment: The Sand

Motor. The Sand Motor is a pilot project involved placing 21.5 million m^3 of sand on the beach and shoreface at the Delfland coast to improve the coastal safety for multiple decades. It's made to supply sediment towards the adjacent coast and dunes by using the natural forces of wind and waves. The Sand Motor not only acts as coastal protection, but the increased beach area and the constructed lagoon have recreational purposes as well. An aerial photo of the Sand Motor, made shortly after the placement was finalized is displayed below (Fig 5).

Figure 5 The Sand Motor in July 2011, just after construction [18]

Since the Sand Motor was the first of its kind, it triggered much scientific interests. This pilot project can be used to gather insight in how mega-nourishments behave and how it feeds sediment to the adjacent coast and dunes.

The design of the Sand Motor was based on a stand-alone hydrodynamic model. This holds that only the subaqueous part of sediment transport is simulated, ignoring the aeolian processes. Separately, the method of De Vriend and Roelvink [31] was used to predict dune growth. The 'Milieu Effect Rapport' Aanleg en zandwinning Zandmotor Delflandse kust (2010) predicted that the Sand Motor would induce a dune growth of 164 to 194% compared with the standard nourishments [21]. However, measurements showed significantly lower growth rates. To prevent waste of (economical) resources and ensure sufficient protection of the hinterland, knowledge about dune development must be improved. A process-based aeolian transport model could help to improve knowledge and reduce flood risk for the future.

1.5 Problem statement

Sea level rise is likely to accelerate. To ensure protection from the water for the hinterland, nourishment volumes need to increase. Mega-nourishments could be the solution. However, aeolian transport of sediment towards the dunes at Mega-nourishments is not yet fully understood. Consequently, there is a large overestimation of predicted dune growth. The design of these Mega-nourishments is crucial in achieving flood protection. Therefore, the most important processes affecting dune growth at nourished coasts must be known. A process-based model could be the next step in improving the current knowledge about aeolian transport. However, this is yet to be tested.

1.6 Research questions

Following the problem statement, the main research question is:

To what extent can dune growth at a Mega Nourishment be predicted by a process-based aeolian model?

Research sub-questions:

1. *What are the natural processes affecting dune growth?*
2. *To what extent can a process-based aeolian transport model simulate the dune development of the Delfland dunes?*
3. *How does an increasing mean sea water level affect dune growth at different coastal profiles?*

1.7 Approach and thesis outline

First, the important natural processes influencing dune growth are identified based on a literature study. Then these processes are implemented into the process-based aeolian model: 'AeoLis' and the model is verified. After verification, the model is applied on a case study: The Sand Motor, from where many bathymetry measurements are available. The measurements are processed to reflect the actual dune growth at the Delfland coast between 2011 and 2020. A hindcast by the AeoLis model, is compared with this measured dune growth to calibrate and validate the software. After validation, multiple water level scenarios are simulated to determine the effect of these water levels and coastal profile on dune growth.

Chapter two contains the literature study. Subsequently, research sub-question 1 is answered. These processes are then, where possible, implemented in AeoLis and a verification is performed. Chapter three contains the case study, which includes the description of the Delfland coast and the model setup. In chapter four, measurement processing and the observed dune growth are presented. In chapter five, a model validation is carried out and research sub-question 2 is answered. The final research sub-question is answered in chapter six, where the influence increasing water levels is determined for different coastal profiles. In the last chapter, chapter seven, the discussion, conclusion and recommendations are presented.

2 Identifying and implementing natural processes affecting dune growth

Based on a literature study, the first section answers the first research sub-question: *What are the natural processes affecting dune growth?* The second section is about implementation of these processes.

2.1 Processes affecting dune growth

Water acts as a transporter of sediment. Wave impact induces shear stresses on the bed resulting in sediment being mobilized. Larger waves exert larger shear stresses on the bed and thus more sediment is set in motion. Mobilized sediment is then dispersed by the alongshore currents. Erosion of the peninsula of the Sand Motor can in this way supply sediment to the adjacent coast. Accretion of sediment can result in larger beach widths and subsequent larger sediment availability for aeolian transport, which is beneficial for dune growth.

Another form of marine transport is cross-shore sediment transport. This process is governed by the balance of forces in the vertical velocity profile. Short waves transport mass towards the shore. When the waves reach the coast, there is confined space resulting in a return flow. This offshore return flow balances the onshore going mass of waves. When extreme wave heights occur, it is possible for the water to reach the dune face. Sediment present in the dunes can then be eroded by the waves, resulting in large dune erosion.

A second transporter of sediment is wind. Aeolian transport of sediment towards the dunes can result in dune growth and increased coastal safety. The amount of aeolian sediment transport is highly dependent of the windspeed. When only accounting for wind capacity, the transportation of sediment at the coast would be overestimated. The wind transportation capacity is only reached when there is sufficient sediment availability. Nourishments tend to widen the beach and therewith increase the sediment availability resulting in larger dune growth. However, there are many sediment availability-limiting factors along the coast. For instance: water, vegetation and sediment sorting.

Figure 6 Dune formation at the Sand Motor (May 2020).

Waterbodies such as the lake and lagoon at the Sand Motor peninsula act as sediment traps since no sediment is able to be transported across. Another effect of water on sediment availability is due to increased moisture content. Wet sand is more cohesive than dry sand, increasing the shear velocity threshold for regions with high moisture content. Particles with larger grainsizes have a higher shear velocity threshold for transportation. Wave runup, capillary rise and soil drying directly influence the soil moisture content.

Vegetation provides shelter from the wind by covering a fraction of the surface and providing a lee-side wake [40] cause disturbances in the flow field, which induces sedimentation. A second effect of vegetation is that it affects wind velocity profiles, by acting as roughness, which results in the growth of a boundary layer downwind [41]. In short, vegetation captures sediment which results in the formation of dunes (Fig 6). Vegetational patches are only found at the supratidal area since wave impact destroys the plants located in the intertidal area.

Sediment sorting can reduce the availability of sediment significantly [20]. Nourishments consist of sand particles and shells of different sizes. Smaller grains with a lower shear velocity threshold are entrained by wind more easily. Therefore, smaller grains are transported where particles with larger shear velocity thresholds remain on the bed resulting in an overall increase of the shear velocity threshold value. Especially shells, which have a high shear velocity threshold, remain on top of the bed (Fig 7).

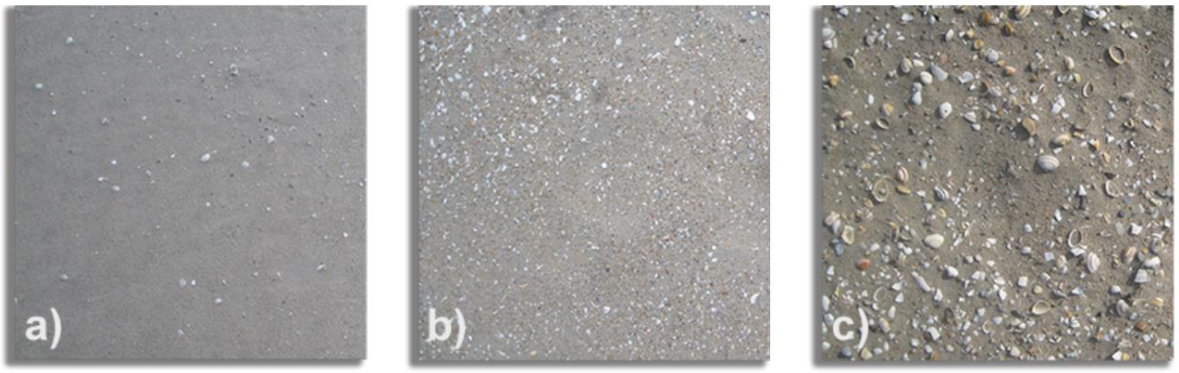

Figure 7 Visual impression of armor layer at three locations in the Sand Motor region: a) intertidal beach, no armoring b) lower dry beach, minor armoring with shell fragments c) upper dry beach, severe armoring with many shells and coarse san d [16].

In the intertidal area, where waves stir up the sediment and induce mixing of the top layer, sediment sorting is countered. This results in larger sediment availability in the intertidal area compared to the supratidal area. However, the increased moisture content in the intertidal area compared to the supratidal area has a reversed effect.

The development of the dunes is linearly dependent on the beach width, as found by De Vriend & Roelvink [31]. First, Greater beach widths provide larger sediment availability. Consequently, larger dune growth is expected. Second, greater beach widths reduce the chance of wave erosion at the dune front since it is less likely for the water to reach the dunes.

2.2 Process-based aeolian modelling

A recent development in aeolian transport modelling is AeoLis. AeoLis is a state-of-the-art process-based model that can simulate aeolian sediment transportation through a domain, where both sediment transport capacity and sediment availability are considered. Therefore, the AeoLis software is chosen to perform the simulations for this research. However, the software is still in development and should be tested to get insight in its strengths and limitations. First testing was done by Hoonhout & de Vries (2018). They found that the AeoLiS model is able to reproduce large scale spatial patterns in aeolian sediment transport in the Sand Motor domain in the four years after its construction [1]. In the following years, further improvements in AeoLis were made.

In this study, AeoLis will be evaluated on smaller scale and for a longer time period. Furthermore, alongshore variation in dune growth was not considered in their study. Alongshore variation is an important aspect in the predictions, since local differences highly influence the effect of natural processes on dune development. Therefore, this study will elaborate on this.

Model implementation

Based on the forcing input, sediment is exchanged between grid cells over time, which results in coastal development. The most important forcing parameter for aeolian models is the wind forcing. The sediment transport capacity of the wind is calculated according to Bagnold's formula [23]. The wind velocity has a large impact on the magnitude of aeolian transport capacity. Since Bagnold executed his experiments in the desert and wind tunnel, where sediment availability does not play a role, this equation tends to overestimate the magnitude of aeolian transport at beaches. To simulate the aeolian sediment transport at beaches more accurately, the sediment availability must be considered as well.

In AeoLis the net sediment entrainment is determined based on the value of the saturated sediment concentration c_{sat}, which is calculated using the empirical formula Bagnold as mentioned above, compared to the value of the instantaneous sediment transport concentration c. The entrainment is maximized by the available sediment in the bed m_a:

$$E - D = \min\left(\frac{\partial m_a}{\partial t}; \frac{c_{sat} - c}{T}\right)$$

Where

T = Adaptation time scale [s]
E = Erosion [kg/m^2/s]
D = Deposition [kg/m^2/s]
t = Time [s]

AeoLis takes aeolian sediment availability limiting processes into account, which influence the m_a value in the prementioned equation. These processes are:

1) Moisture content
2) Vegetation
3) Beach armouring effects due to sediment sorting

Moisture content of a cell is determined based on the geotechnical mass content of water, which is the percentage of water compared to the dry mass. This value is influenced by the groundwater level and capillary rise on the one hand and wave runup, infiltration and evaporation on the other hand. The largest moisture content value is selected per cell [24]. Cells with a moisture content larger than a predefined value have the shear velocity threshold set to infinity. Therefore, wet cells cannot

supply sediment for transportation. The dry time of a cell is determined by the parameter T_{dry} [s] which is the adaptation time scale for soil drying.

Vegetation is implemented as an increased shear velocity threshold for the cells in which vegetation is selected. In this research the vegetation density and growth are set to maximum values to ensure that all sediment is captured in the selected cells and no sediment is transported out of the domain. The selected vegetation cells in the case study are those inside the Dunes polygon, as described in the section 4.1. The amount of sediment passing this vegetational strip is found negligible.

The saturated sediment concentration c_{sat} is calculated for all sediment fractions of the grain size distribution. Smaller grains are entrained more easily than larger grains leading to beach armouring. Consequently, the grain size distributions may vary over time and place in the horizontal grid. To ensure sufficient sediment and allow the model to simulate the sediment sorting process, vertical bed layers are implemented (Fig 8). A minimum of three vertical layers are required. The top layer is the only one that can exchange sediments in horizontal direction. The bottom layer is a base layer that contains an infinite amount of sediment according to the initial grain size distribution. This layer can supply sediment to the layer above. The middle layers (bed composition layers) exchange sediment from the base layer towards the top layer or vice versa. If the top layer interacts with the wind and sediment is eroded, bed composition layer will replete the top layer according to its own grain size distribution. Since smaller grains are entrained more easily, the grainsize distributions of the top layers and therewith those of the bed composition layers, change.

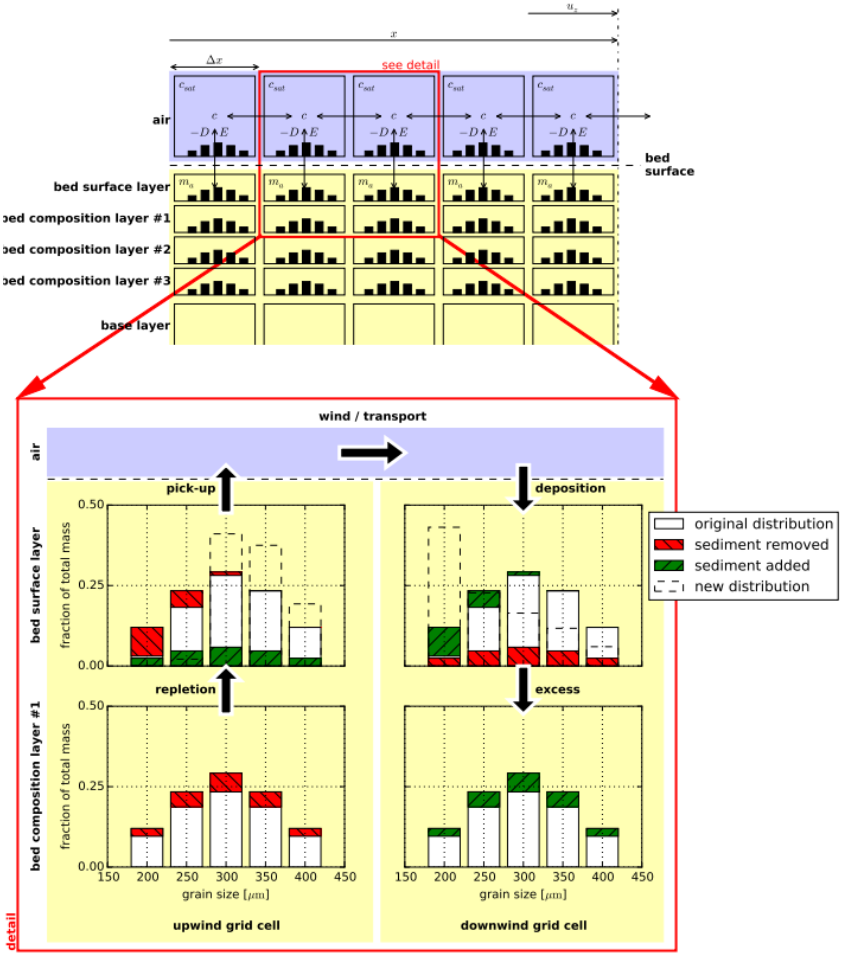

Figure 8 Sediment exchange between horizontal and vertical cells [24].

After implementation of the prementioned processes, a verification was performed.

3 Case study

3.1 Sand Motor

The Holland coast, the coast of the Netherlands between Den Helder and Hoek van Holland, is one of the three parts the Dutch coast is typically divided in. The other two parts are the Southern Delta coast and the Wadden coast. The division is based on the morphodynamic appearance of the coasts. The Holland coast is an 118km long sandy coast that behaves as a beach-dune system. The southern part of the Holland coast is the Delfland coast. The Delfland coast is a coastal stretch with a length of 17 km, reaching from the Hoek van Holland port entrance in the south towards the Scheveningen harbour in the north. In the middle of the Delfland coast lies the Sand Motor: A mega-nourishment constructed in 2011.

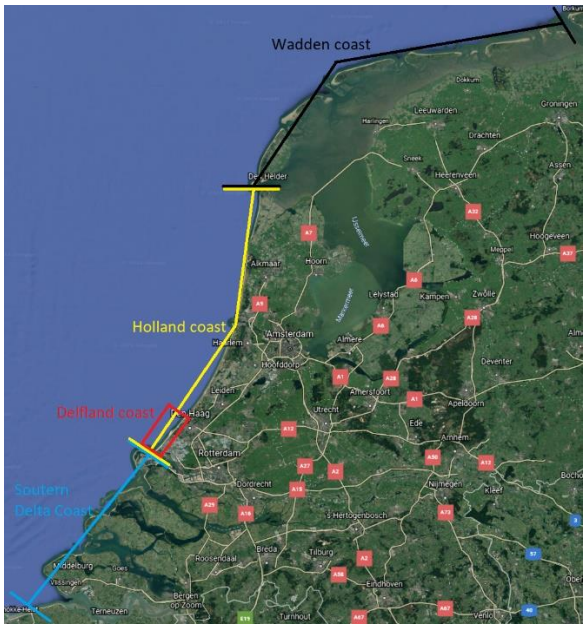

Figure 9 The Dutch coast divided into three parts [22]

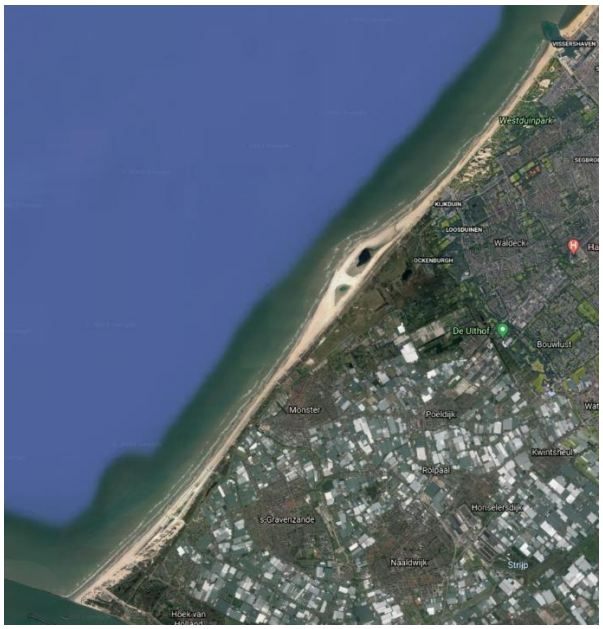

Figure 10 The Delfland domain, with in the middle the Sand Motor[22]

The Holland coast has been suffering from erosion for hundreds of years. Especially in the northern and southern part (Delfland coast) the landward retreat of the shoreline was large. During the period between 1600-1800 the shoreline recession was estimated to be between three and five metres per year and from 1800 onwards between 0.5 and 1.5 metres per year [15]. The decrease in shoreline retreat was due to man-made coastal protection structures like groynes. Nowadays hard structures like groynes are only used to maintain the shoreline if there are no other viable options. In line with the Building with Nature concept as described in chapter one, nourishments, such as the Sand Motor, are preferred.

The Sand Motor is a mega-nourishment, consisting of 21.5 million m^3 of sand on the beach and in the shoreface. It is unique due to its size, design and multifunctionality [26]. The size of the Sand Motor is about five times larger than that of an average nourishment and its aim is to increase coastal safety by feeding sediment to the dunes and adjacent coasts during a period of multiple decades. Next to its safety purpose it has a recreational purpose as well. The peninsula increases the beach area and the lake and lagoon are often used by surfers and for other water-activities. The lagoon area was also expected to have environmental benefits, increasing the population of fish and birds. The larger volume of the nourishment, which reduces the nourishment frequency, has ecological benefits as well.

3.2 Model setup

In this section, the chosen model setup variables are described.

Bathymetry

For the simulation, the same bathymetry and polygons are used as for the measurements. Since there is no subaqueous spreading of sediment of the peninsula to the adjacent coasts, there are no large changes in the bathymetry during the simulated period.

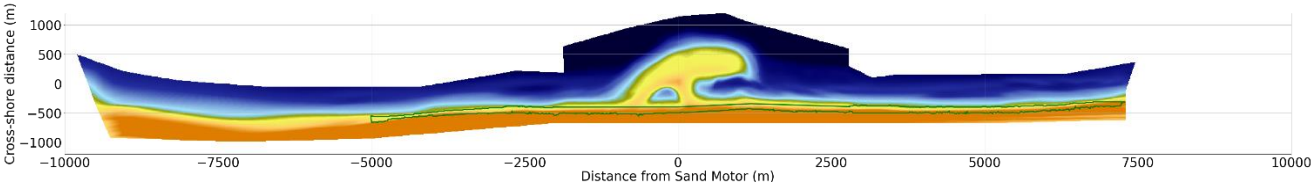

Figure 11 Bathymetry used for Aeolis simulations of the Delfland domain. Dune polygon is indicated in green.

Grid

The optimal value for grid cell size is determined to be 20m x 20m. Smaller grid cells currently result in a disproportionate increase of computational time. Larger grid cells result in lower resolution and less accurate simulations.

Initial conditions

For the initial state, the bathymetry is used as measured in August 2011. A strip of vegetation is modelled from the dune foot landward. This stroke has maximum density and growth speed to make sure all sediment transported landward is captured in the dunes instead of being transported over the domain's landward boundary.

Contrary to the sea, no waves and tidal variation are present in the lake. In the lagoon there is less tidal variation and limited wave and runup heights. To simulate these effects, wave, tide and runup masks are applied.

The ground water level around the lake and lagoon was found to be around 2.0m higher than the mean sea water level (MSWL), see appendix B. This increased water level is included in the tide mask.

Boundary conditions

Constant zero flux offshore and onshore boundaries are used, which means that no sediment is going into the domain through the offshore and onshore boundaries. The lateral boundaries are circular boundaries.

Forcing conditions

Wind conditions as measured between 2011 and 2020 are used in the simulation (Fig 12). For the tide, the water levels measured at the Europlatform in 2011 are used and repeated over the simulated years. The waves are simulated as standard waves of 2m height and a period of 5s. Additional simulations showed that the simulation outcomes are not sensitive for small wave height and period deviations.

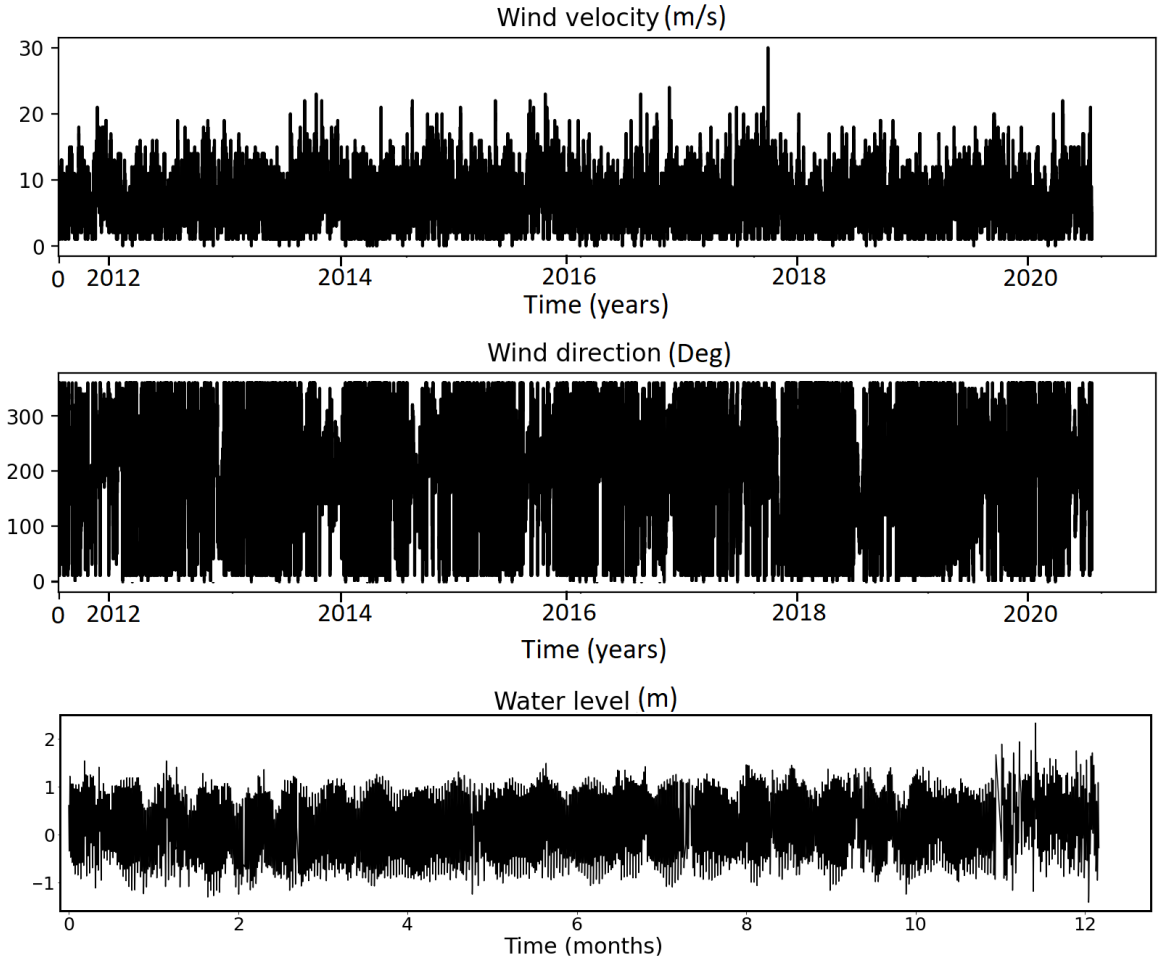

Figure 12 Forcing conditions used in the Aeolis simulations. Water levels are repeated over the duration of the simulation.

Parameter settings, masks, & enabled Processes

A full list of used parameters, masks, and processes is given in appendix A.

Limitations and assumptions

The reference simulation is made to resemble the situation of the Delfland coast between 2011 and 2020 as accurate as possible. This way, the model's performance can be assessed based on the measurement results. The current limitations of the model are to be described in this section. From these limitations several assumptions are made. Since the JETSKI and LIDAR campaigns (section 4.1) did not measure the whole original Delfland coast, just after the construction of the Sand Motor was finished, JARKUS data [39] is used to form the initial bathymetry as used in the model. This data has a much lower resolution than the LIDAR and JETSKI data, therefore the initial bed as used in the model is likely to somewhat deviate from the real bathymetry at that time.

Another difference between the initial modelled situation and the one in reality is the (armoured) state of the coast. The model starts with an unsorted grainsize distribution for the whole domain. This holds that during the first year an increased transport volume is expected, since no armouring

effects play a role. In reality, the Sand Motor was not constructed in one day. Consequently, armouring effects already took place during construction. When the Sand Motor was officially finished constructing, the major part of the peninsula was already armoured. The increased transport rate during the first year is expected to be smaller than in the model.

The limitation with the largest impact is the lack of marine transport in the model. This holds that there is no addition, rearranging or erosion of sediment in the shoreface. The system, as defined by the user, cannot find a new equilibrium as it would in reality. Especially after nourishments, where an intervention in the system is made, there is much subaqueous transport which results in a new situation. The simulation of the Delfland domain, where the construction of the Sand Motor has a large impact on the development of the (subaqueous) coastal profile, can therefore not completely match the measurements. To cope with this model limitation, in terms of alongshore dune growth variation, only results of the first two years after construction of the Sand Motor are compared with the measurements. After two years, the discrepancy between the model's bathymetry and the reality becomes too large. These years are not taken into account.

The lack of marine transport does not only result in different behavior in the intertidal area, the dune front is affected as well. No wave-erosion module is present. This holds that the volume of the simulated dunes can only increase over time. In reality an equilibrium beach width is found for the Holland coast of 115m [31], when wave erosion of the dune front and aeolian sediment transport towards the dunes are balanced.

To prevent sediment from leaving the modelled domain, a large vegetation stroke is placed in the Dune polygon. This vegetation has maximum density and grow speed which holds that it remains in place over time and does not let sediment pass in landward direction. In reality, dune development is a far more complex process but it is assumed that this simplification does not result in different sediment transport volumes.

The lack of marine transport results in no addition or rearranging of the sediment in the coastal profile. Aeolian transport results in lowered bed levels just above the shoreline, where the (dry) sediment is prone to transport. Since there is no rearranging of sediment, this bed level is lowered until the cell becomes flooded. Consequently, the boundary between the intertidal and supratidal area moves landward over time. This landward moving shoreline is seen in reality as well, though with a smaller magnitude [12]. This faster landward moving shoreline in the model is assumed to be compensated in this study by taking a time-averaged width of the intertidal and supratidal zones. This way, the sediment flux proportional to the beach width remains approximately equal. However, in absolute sense, there is an underestimation of the sediment flux in the model compared to the measurements.

Another way to cope with this faster landward moving shoreline is to enable the process 'wet bed reset'. This adds sediment to the flooded grid cells, to restore the initial bed level, based on a predefined timescale. Simulations with this process enabled did not result in notable differences in outcome (appendix B).

4 Measurements

This chapter describes how the measurements are processed and then shows the observed dune growth of the Delfland domain.

4.1 Measurement processing

Since the Sand Motor is the first mega-nourishment in the world, extensive measurements are taken to monitor its development. Measurement were carried out between 2011 and 2020. For this, multiple measurement techniques are used. In the first year, monthly measurements of the beach dunes and subaqueous part of the domain are taken using a jet ski, quad bike, and GPS on a wheeled pole [30]. After one year the interval of these surveys was reduced to once every two months. This monitoring campaign is called JETSKI. For more accurate measurement of the dry part of the domain, LiDAR images were taken with an unmanned aerial device (UAV). These images contain a higher resolution than the JETSKI measurements. These images are not accurate for the wet parts of the domain and can only be used for bed level changes of the dry parts. These surveys are executed twice a year.

The JETSKI and LIDAR data is processed to be able to assess the development at the Delfland coast. A bathymetry measurement for both the JETSKI and LIDAR campaigns consists of many measurement points (Fig 13). Every point consists of a X, Y and Z coordinate. A grid of 10m x 10m is formed over the research domain and for every grid cell an interpolated bed level is calculated based on the measured coordinates. For a more extensive description of the measurements see [17] [19]. For visualization purposes, the axes are rotated by 50 degrees. The left-hand side of the plot is the southern side of the domain.

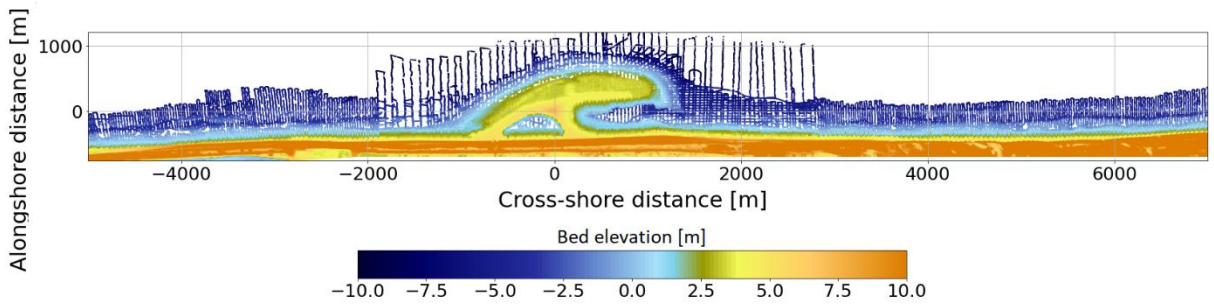

Figure 13 LIDAR and JETSKI measurement points combined and rotated, measured in August 2011.

Design coastal indicators

Coastal indicators can serve as a tool to assess the morphological behavior of a coastal stretch, which is helpful for observing trends and predicting future development. The following two coastal indicators are selected to assess the influence of the Sand Motor on the Delfland coast and evaluate the model's results:

- Integrated dune growth
- Alongshore variation in dune growth

To compare the integrated dune growth at the pre-existing beach with the dune growth at the Sand Motor, the Delfland domain is split in two parts. The Regular coast domain and the Sand Motor domain (Fig 14). For the alongshore variation in dune growth, alongshore widths of 10 meters are used.

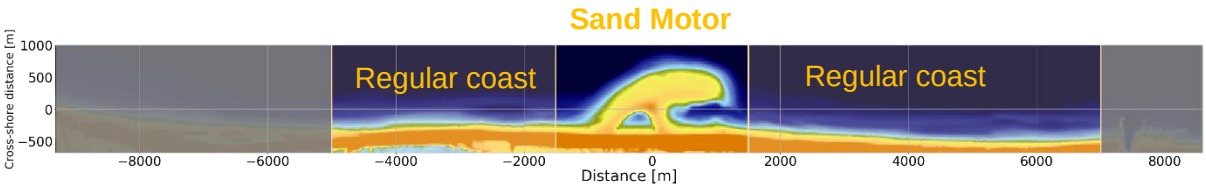

Figure 14 Split between Regular coast and Sand Motor sections

To evaluate the development of these coastal indicators, the Dune polygon is specified (blue line Fig 15). In this polygon bed level changes over time are determined in order to calculate the sediment flux towards the dunes. The lower line of the Dune polygon is located at the 3m NAP line, where the dune foot is usually defined. The upper line of the Dune polygon is determined based on local variability of the dune height. For every ten metres in alongshore direction a point in cross-shore direction is determined where the variance of the dune height variability over time is less than the set threshold of 0.01m. Connecting those points results in the upper line of the polygon. The amount of sediment passing this line is assumed negligible. The southern (left) boundary of the polygon is limited at the Spanjaards Duin, where human activity impacted the measurement results. The northern (right) boundary of the polygon is limit at the Scheveningen harbor. The dark grey areas indicate the location of the sedimentation between 2011 and 2020 (Fig 15).

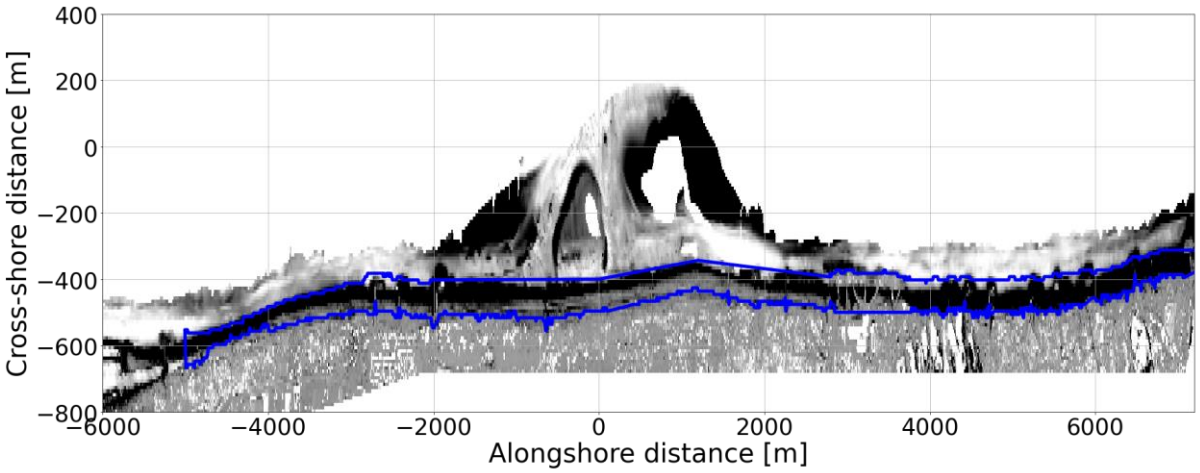

Figure 15 Dune polygon and sedimentation location. Note that the y-axis is stretched to improve the view of the Dune polygon's location.

4.2 Observed dune growth

Despite the large peninsula at the Sand Motor domain, the measured dune growth is 29% less than at the regular coasts (Fig 16). A nearly linear trend is observed for the dune growth over time. The increasing gap in dune growth volume between the Regular beach and Sand Motor may be explained by the armouring effects taking place at the Sand Motor. The nourished sediment present in the Sand Motor domain contains shelves and other large particles, causing an increasing shear velocity threshold over time. These particles are not present at the regular beaches. In the Sand

Motor domain, most of the sediment originates from the intertidal area [38], where armouring effects play no role.

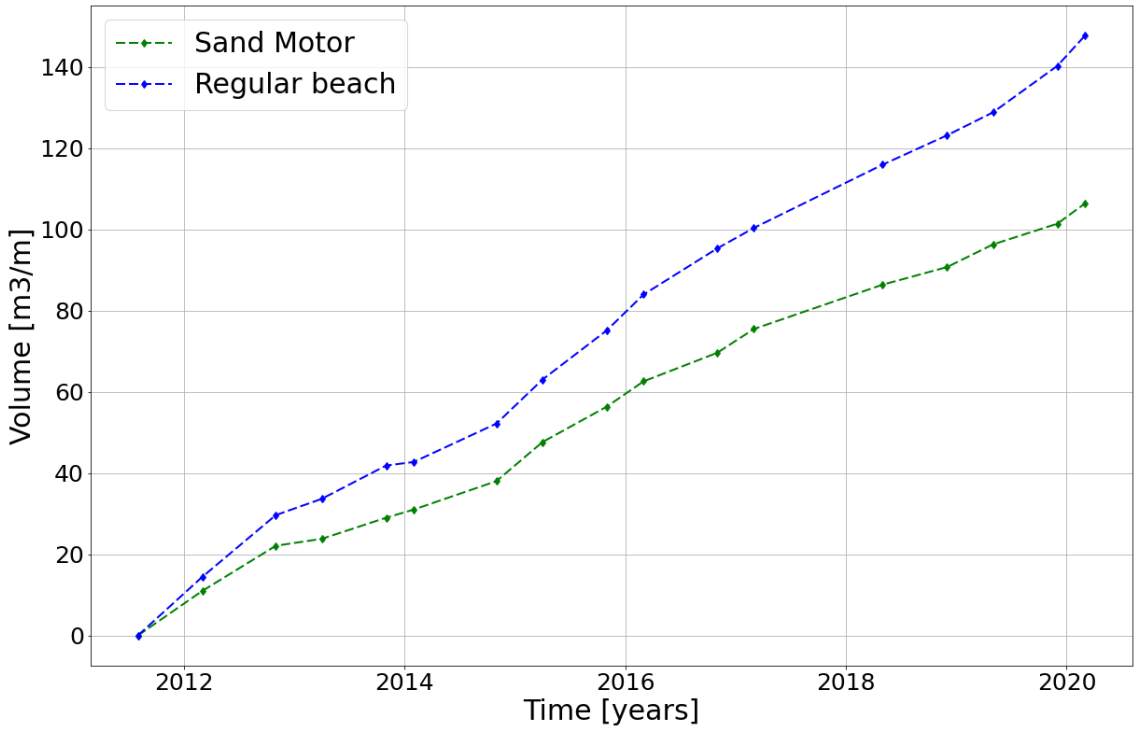

Figure 16 Dune growth over time for the Sand Motor domain (green) and the regular beach domain (blue). Measurement dates and volumes are indicated with diamonds.

Alongshore dissimilarities in coastal profile cause differences in dune growth. Previous studies found that the magnitude of this flux is positively correlated to the beach width [31][29]. Since the construction of the Sand Motor greatly increased the beach width at the peninsula, large dune growth was expected [21]. However, the dunes in the lee of the peninsula experienced less growth than the dunes behind the regular beaches. Hence, the influences on dune growth are analyzed.

Three sections are selected based on coastal profile and grainsize distribution (Fig 17). The area between section 2 and 3 will not be considered since human interference around Kijkduin caused deviations in the measurements**.**

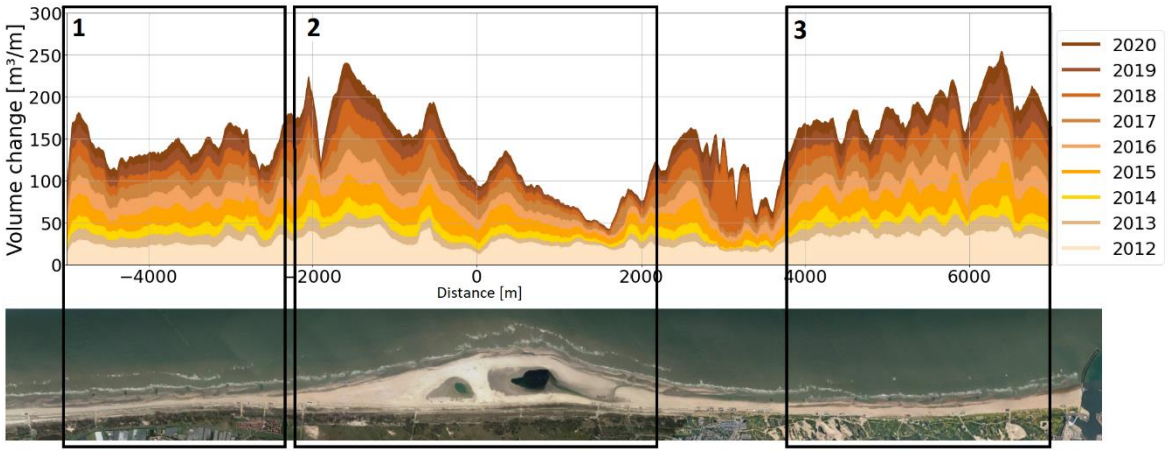

Figure 17 The upper graph shows the alongshore dune growth variation in the Delfland domain during 2011-2020. Tints indicate the growth during specific years. The lower figure shows an image of the Delfland domain in 2020, corresponding to the alongshore

The dunes in section 3 experience in average 21% more growth than in section 1 (Fig 17). This difference can be explained by the beach width. The beach width is positively correlated to the sediment flux into the dunes in the lee of that beach [29] and the beach in section 3 is wider than in section 1 (Fig 17). Direct influence of the Sand Motor can be ruled out since these section locations are too far from the peninsula.

There is a large variation in alongshore dune growth in section 2, where the lake and lagoon are of large influence [38]. Their positions are highlighted in green and blue (Fig 18).

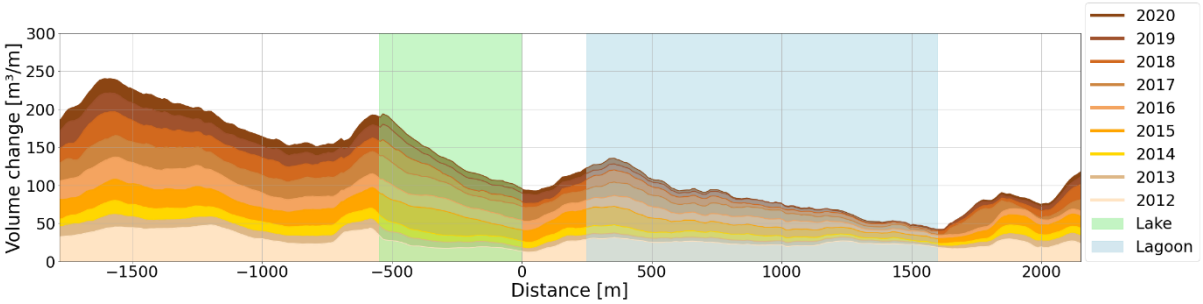

Figure 18 Zoomed-in view of zone 2 indicated in figure 17. Highlighted in green and blue are the alongshore length of the lake and lagoon respectively.

The dunes in the lee of the Sand Motor experience the least growth of the entire domain. This can be explained by the presence of the lake and lagoon, which act as sediment traps.

Starting from the southern side of section 2, an increasing effect of these traps is expected due to the decreasing effective beach width. This would result in a more or less linear decline in dune growth towards the north. Two significant exceptions can be seen. The first one around -550m and the second at 400m (Fig 18). The peak at -600m is partly explained by human interference in the dune system during the construction of the Sand Motor (Appendix C). It took years for the nature to restore the hole in the dunes that was dug for constructional purposes. The second peak, at 400m, is explained by the supratidal area between the lake and lagoon. For specific wind directions, sediment originating from the peninsula head can still accumulate at the dunes.

Another explanation for the decreasing dune growth is that the largest part of the sediment supply towards the dunes originates from the intertidal area [38]. Behind the lake and lagoon there is no intertidal area. Absence of tidal mixing of the sediment results in less dune growth.

The least dune growth of section two is found around 1500m. This can be explained by the earlier mentioned effects combined with the smallest effective beach width of the section.

5 Model performance for predicting multi-year dune growth

In this chapter, the second research sub-question will be answered: *To what extent can a process-based aeolian transport model simulate the dune development of the Delfland dunes?*

5.1 Integrated dune volume

For the integrated dune volume over time, the domain is again divided in two parts: The Sand Motor and the Regular beach. The Sand Motor domain consists out of nourished sediment (Fig 19, green line). For the regular beach domain, a simulation with the in reality present grainsize distribution is made (blue line) and a simulation with nourished sediment distribution is carried out as well (red line). An initial shelfs content of 5% induces an ultimate reduction of the sediment flux of 54% (red and blue lines). When not accounting for the first half-year, where both scenarios with and without shelfs behave approximately the same, the sediment flux is reduced by 62%.

The measured integrated dune volume change does not show a fast-initial growth such as shown by the model. This primary overestimation of the sediment flux towards the dunes is explained by the initial conditions of the model, as described in 3.2 Since the Sand Motor took almost a year to construct, an armoured layer was likely already developed on large part of the peninsula when the first measurement took place in august 2011. Also, the neglection of rainfall in the model plays a role in the coastal development. Rainfall increases the moisture content, which decreases the sediment availability and therewith the total transport. Consequently, the extreme transport rates simulated in the first half-year would likely to be flattened out and the armouring processes would be slowed down. The previously named effects combined could explain the difference between the measured and modelled first half year.

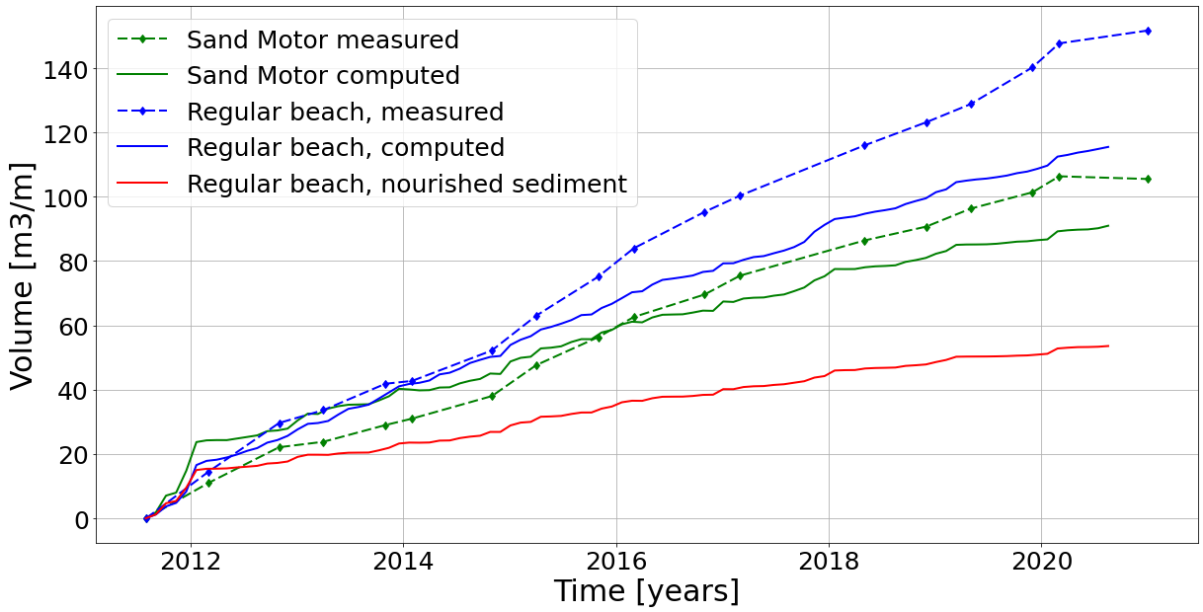

Figure 19 The integrated dune growth between July 2011 and October 2020. The blue and green, striped lines indicate the measured increase in dune volume and the solid blue line and green lines indicate the dune growth predicted by Aeolis. The red line represents the simulation of the regular beaches consisting nourished sediment. The diamonds plotted in the striped lines indicate the measurement dates.

At the Sand Motor domain, the model shows an ultimate underestimation of the sediment flux towards the dunes of 15%. At the Regular beach domain, the simulation without armouring shows an ultimate underestimation of 24%. These underestimations could be explained by the absence of marine transport and the subsequent morphological change. For instance, the spreading of the peninsula's sediment to the adjacent coasts increases sediment supply at the regular beach domain whereas in the model no such behavior is simulated. Another reason for the underestimation in both the Sand Motor and regular beach domains, is the fast-landward moving shoreline in the model, as explained in section 3.2.

At the regular beach domain with nourished sediment, where an initial 5% of shelves is present, the total reduction of dune volume increase after ten years is 54% with respect to the non-armoured beach. This difference in sediment flux remains approximately equal during the final 9 years of the simulation, when the armoured state of the coast is reached.

Another point of interest is the first-year behavior of all the simulations (Fig 20). From July 2011 until approximately the end of the first winter, February 2012, there is a significantly larger increase in dune volume than during the remaining of the simulation.

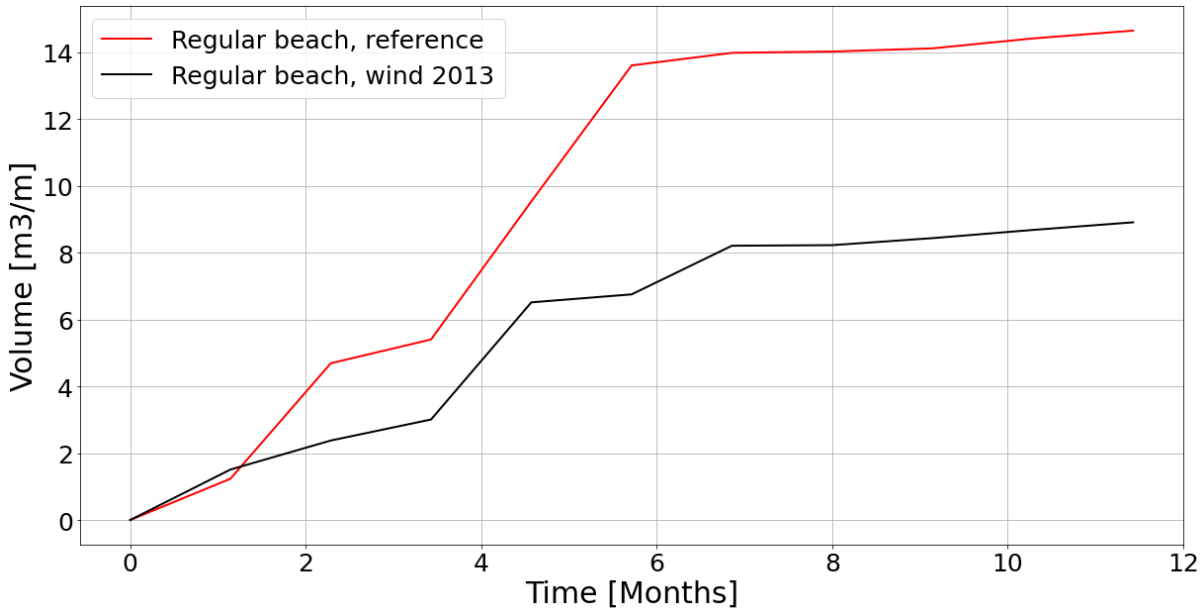

Figure 20 First-year computed dune development with different wind forcing conditions. The red line represents the reference simulation (Fig 19, nourished sediment). The black line represents a simulation starting with wind forcing as measured in 2013, ceteris paribus.

A simulation starting with the wind conditions of 2013 instead of the 2011 conditions, shows a 48% reduction of the dune growth during the first 6 months (Fig 20, black line). This leads to the assumption that the extreme dune growth in the first year is caused by the wind conditions of late 2011, where more extreme windspeeds occurred than during 2012. A second explanation for the extreme volume increase in the model, is the initial bed composition. The bed consists 5% out of shelves and other large particles which are not susceptible to aeolian transport. This percentage of shelves increases over time (armouring) which increases the shear velocity threshold. After the first half year, the shelves content stabilizes somewhat for the remaining of the simulation.

5.2 Alongshore variation dune development

The assessment of alongshore variation in dune growth, simulated by the model, is based on multiple years. The first three years after construction, starting in the summer of 2011, are evaluated as well as the year 2019-2020. During the first years, the morphological differences between reality and model are still relatively small, which results in smaller deviations in dune growth predictions than for the last year. This shows the importance of a hydrodynamic module to keep up with the morphological changes caused by subaqueous sediment transport. Two specific sections are chosen for comparison of the model computations with the measurements; the Sand Motor domain and the regular beach domain (Fig 21). In these sections, the mean dune growth and alongshore variability in dune growth will be evaluated.

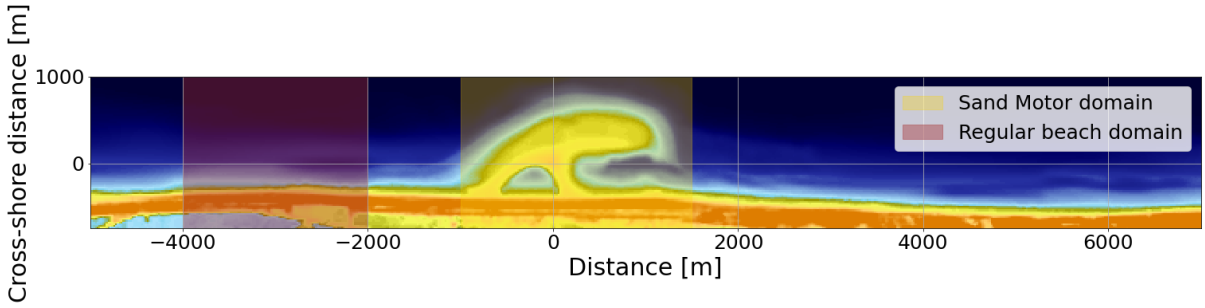

Figure 21 Top view of the Delfland coast. Regular beach domain and Sand Motor domain are incdicated in brown and yellow.

Average dune growth

In the first year, within the boundaries of the Sand Motor domain, AeoLis predicts an alongshore average dune growth of 25.2 m^3 /m (Fig 22). The measurements inside this domain show an average dune volume increase of 25.0 m^3/m. The computed mean dune growth during the two following years is close to the measured growth as well. In 2012-2013 there was only a 2% underestimation of the dune growth and during 2013-2014 the computed dune growth was 12% less than measured (Fig 22). Even during the last year, when significant changes in the morphology at the Sand Motor have taken place, there is only an underestimation of the mean dune growth of 18%. A reason for this high accuracy is that most of the model's parameter settings are calibrated on the integrated sediment flux in the Sand Motor domain [1].

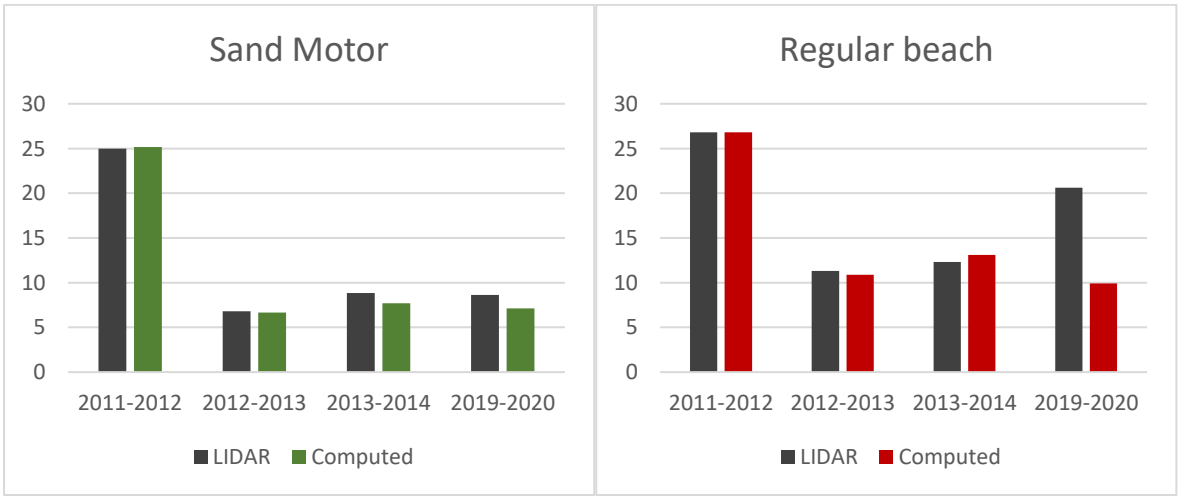

Figure 22 Computed and measured average dune growth [m^3/m] in Sand Motor and regular beach sections during specified years.

In the regular beach domain, where no non-erodible particles are present, the accuracy is approximately as high as in the Sand Motor domain. This is remarkable since no extra calibration was carried out for this section. Except the bed composition, the same settings are used as for the Sand Motor domain. The year 2019-2020 is an exception on the high accuracy of the model. At the regular beach the measured dune growth is twice as high as simulated. This can be explained by the morphological change of the regular beach section in reality versus the change that took place in the model.

In reality the sediment placed at the peninsula head is transported by the waves and currents towards the adjacent coast. This 'feeding' of the adjacent coasts results in a somewhat stabilized shoreline. In the model, there is no subaqueous sediment transport. Consequently, sediment transported out of the intertidal area by aeolian forces is not compensated by marine transport. This causes the shoreline to retreat over time, resulting in a decreased beach width (Fig 23). Since beach width and dune growth are positively correlated [31], the simulated dune growth is expected to be smaller than measured.

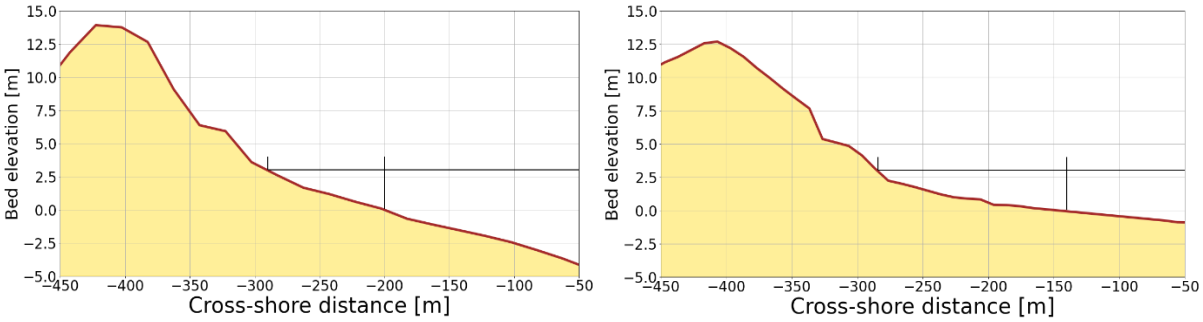

Figure 23 Cross-shore section of the regular beach domain in 2019. LHS is computed, RHS is measured. Beach width is indicated by the black line starting from the dune foot at +3m until the low water line.

The large reduction in dune growth between the first year and the remaining years (Fig 22) indicates the influence of armouring on the sediment flux towards the dunes. In the initial state, the bed

contains 5% non-erodible particles. The rapid percentual increase of these particles (Fig 24) result in less sediment availability and an increased shear velocity threshold.

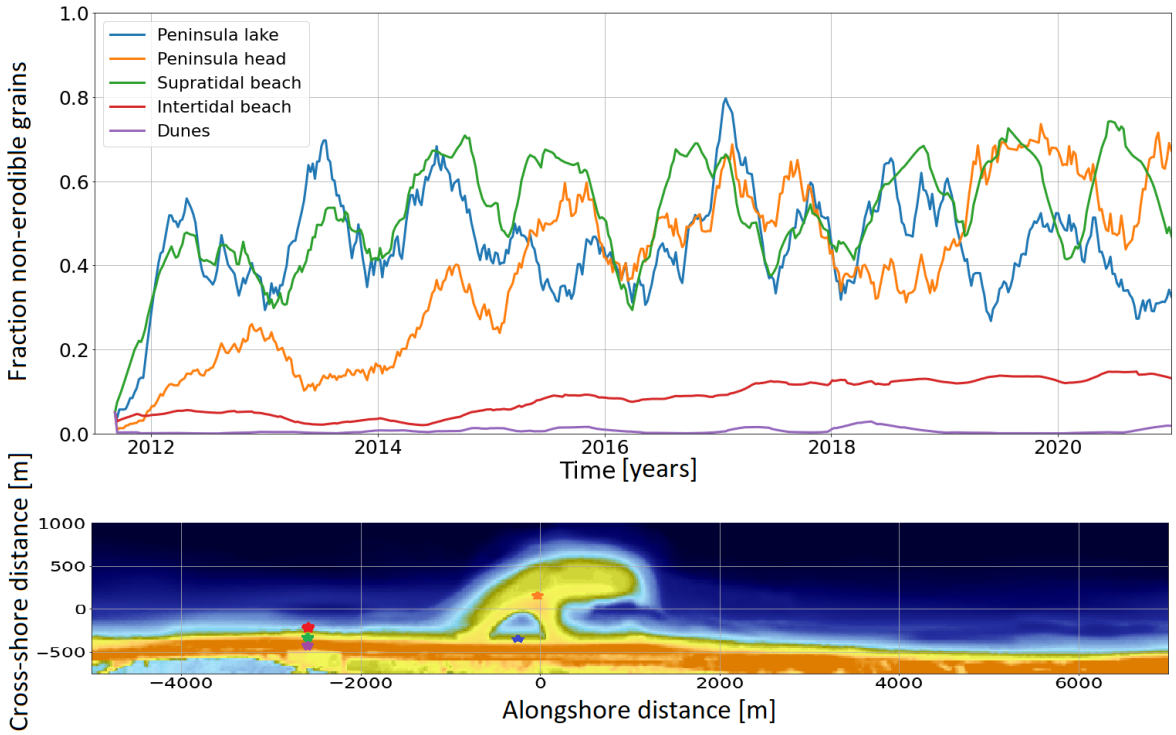

Figure 24 Fraction of non-erodible grains present in the bed over time (upper plot) for specific locations, which are indicated in the lower plot. For every location, compositions of multiple adjacent grid cells are averaged to cope with large jumps in the functions.

Behind the lake the development of the non-erodible particles over time is comparable with in the supratidal area. Both locations are in the lee of a water body. When the wind is coming from the sea (dominant direction), there is zero aeolian sediment saturation at the shoreline so much fine sediment is being picked up just after the shoreline. The non-erodible particles are not transported so during the first few months, when fine sediment availability is still high, there is a rapid increase in the fraction of non-erodible grains in the lee of the lake and at the supratidal beach. At the peninsula head, which is located further from the shoreline, the air is already (partly) saturated with sediment. Consequently, less sediment is picked up and the percentual increase in non-erodible grains is lower. Over time, when the sediment availability between the shoreline and the peninsula head decreases due to armouring, an increasing amount of sediment is picked up at the peninsula and the fraction of non-erodible grains increases. The maximum percentage of non-erodible grains in a bed lies somewhere around 80%. Sheltering of finer grains underneath larger particles cause this maximum.

At the dunes, all aeolian transported sediment is captured. Therefore, the fraction of non-erodible particles remains low. At the intertidal area, there is no such increase found as at the supratidal area. This is explained by wave induced mixing of the sediment, which causes the original composition to be restored.

Alongshore variability in dune growth

For a more detailed analysis of the model performance, the alongshore variability is evaluated. For all prementioned years, an alongshore dune growth plot is made in which the computed transport can be compared with the measured values. Since no armouring processes take place on the regular beaches, a simulation without large particles is plotted as well (Fig 25, red line). The measured dune

growth (Black line) inside the Sand Motor domain (Fig 25, yellow shaded) is compared with the model including non-erodible particles (Green line). In the Regular beach domain (Fig 25, brown shaded), the measured dune growth is compared with the simulation without the non-erodible particles (Red line). This way the model's performance can be evaluated more realistically.

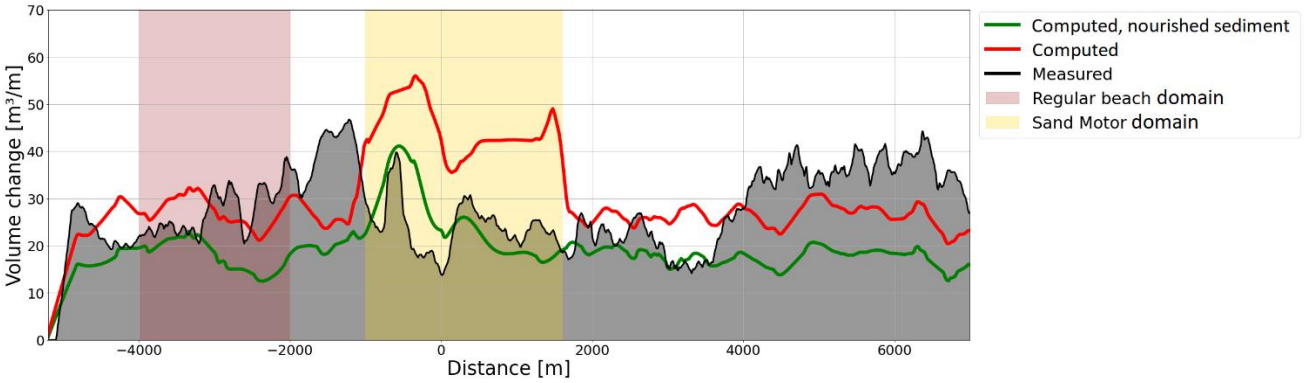

Figure 25 Alongshore dune growth variation in 2011-2012. Measured values are indicated in black, computed values are indicated in red (without non-erodible particles) and green (including non-erodible particles).

The larger beach width around the peninsula induces a larger dune growth than at the regular coast in both simulations [31]. The presence of the lake and lagoon are reflected by the dips around 0 and 1000m, which is in line with the findings of Hoonhout & De Vries [1]. Furthermore, the alongshore trend of the simulations with and without non-erodible particles have similar alongshore dune growth patterns. This is as expected because there is only a decreased sediment availability and increased shear velocity threshold between those simulations, resulting in less transport overall but not in large differences in alongshore pattern.

To assess the performance of the model regarding alongshore variation in dune growth, the variability is calculated (Fig 26). This is done by taking the average of the differences between the dune growth every 20m alongshore and the mean dune growth of that specific section.

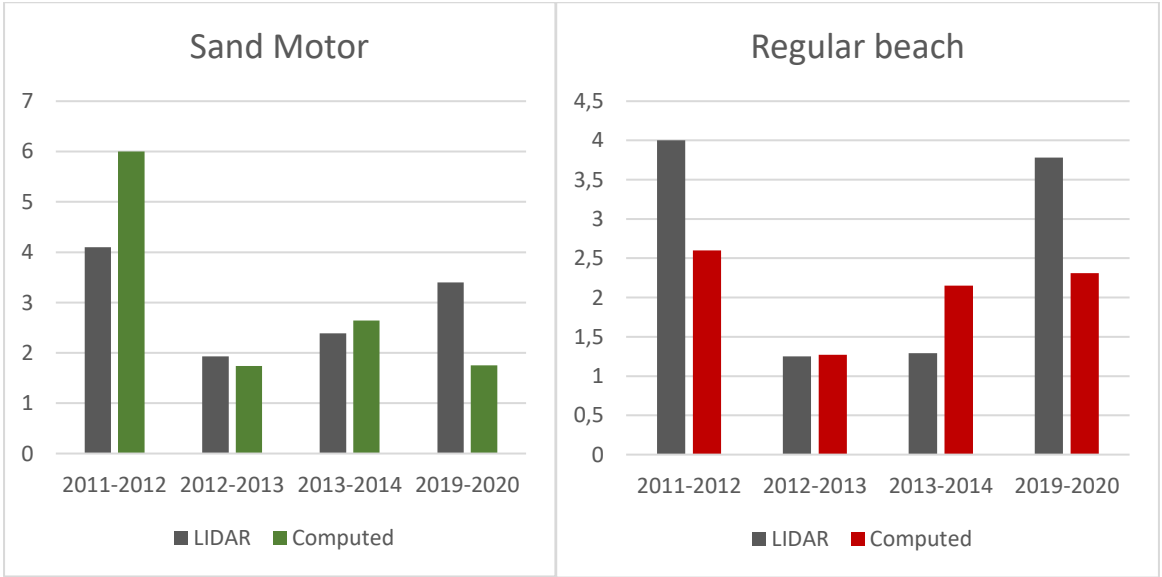

Figure 26 Computed and measured alongshore variability in dune growth in m³/m, for the Sand Motor domain and regular beach domain, during the specified years.

In the Sand Motor domain, the computed alongshore variability in dune growth during the first year is determined to be 6.0 m³/m (Fig 26), which is larger than the measured value of 4.1 m³/m. This overestimation could be explained by the differences in sediment availability. In the model, only 5%

of non-erodible particles are present in August 2011. In reality, armouring processes already took place during the construction of the Sand Motor, especially the area south of the lake, which was constructed early. Consequently, during the first year there is larger sediment availability in the model than in reality. This leads to a large peak in dune growth (Fig 25, -600m) and the subsequent increased variability.

In the regular beach domain, the measured alongshore variability in dune growth during the first year is determined to be 4.0 m^3/m. Contributions to this variability are for instance beach clubs and walkways (Appendix C), which are shown by the peaks and dips (Fig 25, black line). There are no such disturbances of aeolian transport incorporated in the model. However, variations in cross-shore position of the dune foot over the length of the domain causes shadow-effects in terms of accretion at specific locations. This contributes to the computed variability in dune growth, which is determined to be 2.6 m^3/m.

A similar figure as 25 has been made for the second, third and final year of the simulation (Fig 26). This gives insight in the change in accuracy of the model over time. It's expected that due to the lack of marine transport (section 2.1), errors between model and measurements will increase over time. This is also shown by the differences in variability during the last year (Fig 26).

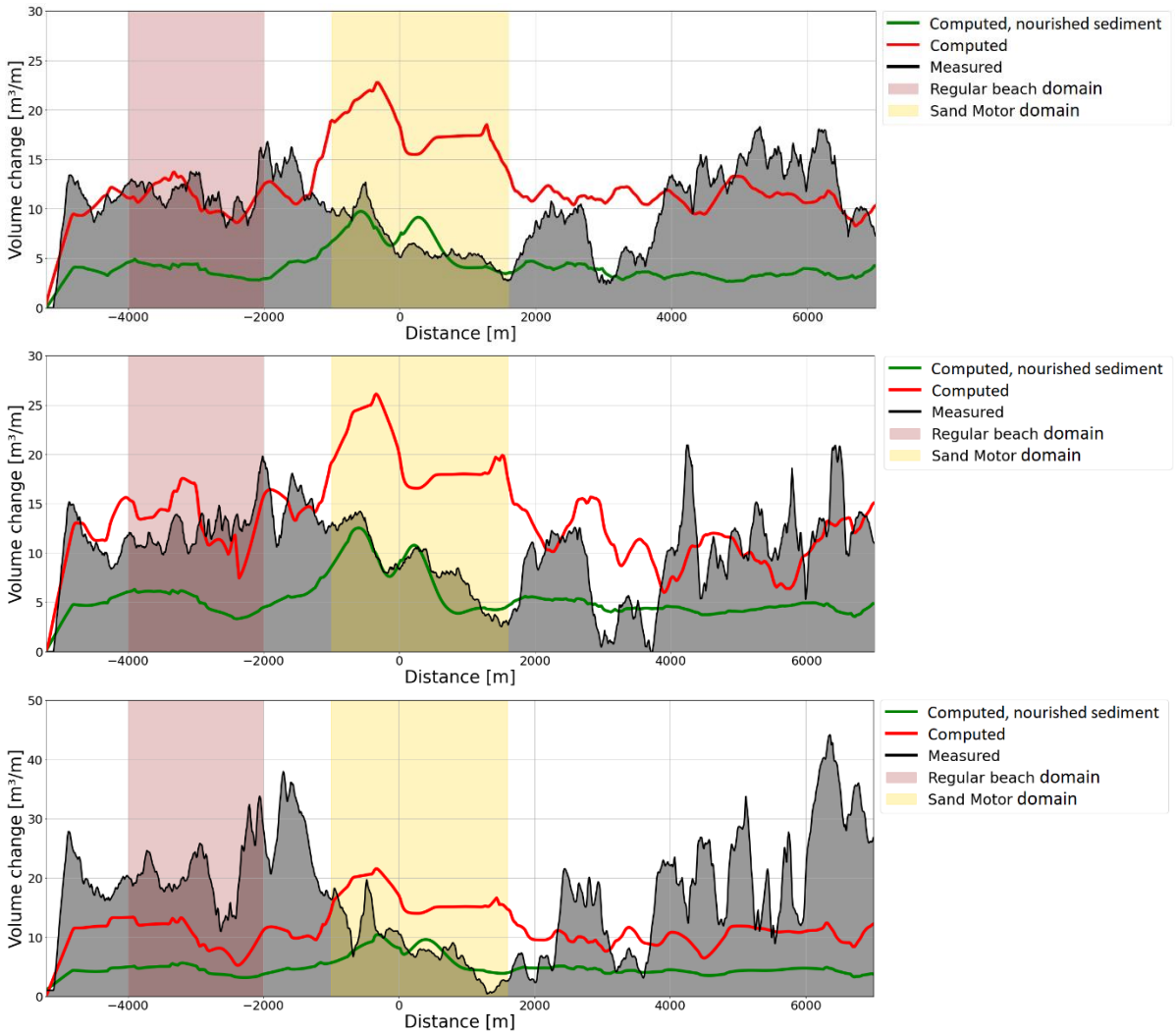

Figure 27 Alongshore dune growth variation in 2012-2013, 2013-2014 and 2019-2020 (top to bottom). Measured values are indicated in black, computed values are indicated in red (without non-erodible particles) and green (including non-erodible particles).

Although there is no large change in the computed alongshore dune growth pattern over time, there is a large reduction of dune growth compared to the first year. The computed dune growth found at the regular beach domain stabilizes after the first year to around 10 m^3/m (Fig 27). The same holds for the Sand Motor domain, where the computed dune growth remains around 7 m^3/m. The measurements, however, show an increasing dune growth at the regular beach domain during the last year compared with previous years. This could be explained by the feeding of sediment by the Sand Motor towards the adjacent coasts, which increases the sediment availability.

6 Impact of increasing water levels on dune growth

In this chapter, the model is used to get insight in how different water levels influences the sediment flux towards the dunes. First an analysis is made for the regular coast, then the Sand Motor coast is analyzed. Linear relations between beach width and sediment flux are expected [31]. The final research sub-question will be answered: *How does an increasing mean sea water level affect dune growth at different coastal profiles?*

6.1 Water level scenarios

Approach

As stated in chapter one, the magnitude of future sea level rise is uncertain. To cope with this uncertainty, different water level scenarios are researched. The reference simulation as discussed 3.2., is used to assess the different scenarios. Due to lack of subaqueous sediment transport in the model, as no marine processes are captured, and the inherent loss of accuracy regarding the dune development, 10-year simulations are carried out. To create a wide range of results, 7 simulations are carried out with a MSWL between -1.0m NAP and +2.0m NAP with incremental steps of 0.5m (Table 1). No sea level rise rate is implemented in the model because the effects on a 10-year timescale were found negligible compared to the influence of the instantaneous increase in MSWL. The starting bathymetry of the simulations is based on the Delfland coastal profile as measured in 2011, just after the construction of the Sand Motor. Dependent on the simulation, there is an instantaneous MSWL increase over the domain, which results in differences in intertidal and supratidal area between the scenarios.

For the model evaluation, the domain is split in two parts, Regular coast and Sand Motor. In the assessment of increased MSWL, three specific sections are chosen (Fig 28). First, a wide and flat regular coast profile. Second, the non-linear Sand Motor profile. The third profile is a small and steep regular profile. These three sections are chosen based on the largest variability between sections in the Delfland domain. This way, the influence of variations in MSWL, and the corresponding changes in sediment transport towards the dunes can be assessed for varying coasts.

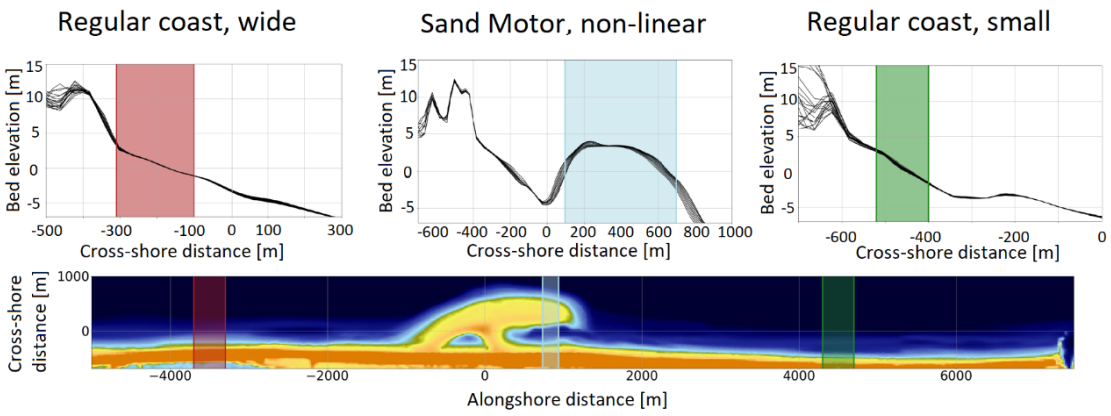

Figure 28 Selected coastal profiles. The lower part shows the location of the sections in the Delfland domain. The upper part shows the cross-shore profiles for the selected section. For every 30m alongshore, a cross-shore plot is added, resulting in the black contours.

There is little variation in dune profile inside a selected section (Fig 28). The highlighted section in the cross-shore plots represents the area susceptible for aeolian transport. For the regular coasts, this section is limited at the LHS by the dune foot and at the RHS by the low-water line. For the Sand Motor coast, this section is limited by the low-water line at the RHS and is limited by the water level in the lagoon at the LHS. The lagoon acts as an artificial vegetational stroke where sediment is being captured and no sediment can be mobilized.

Intertidal and supratidal area

To be able to separately assess the influence of the inter and supratidal area, the high and low-water lines are determined (Fig 29). The mean peaks and lows during that year are determined, resulting in the upper and lower red lines. The high-water line is determined at 1.68m, the low-water line at 0.08m.

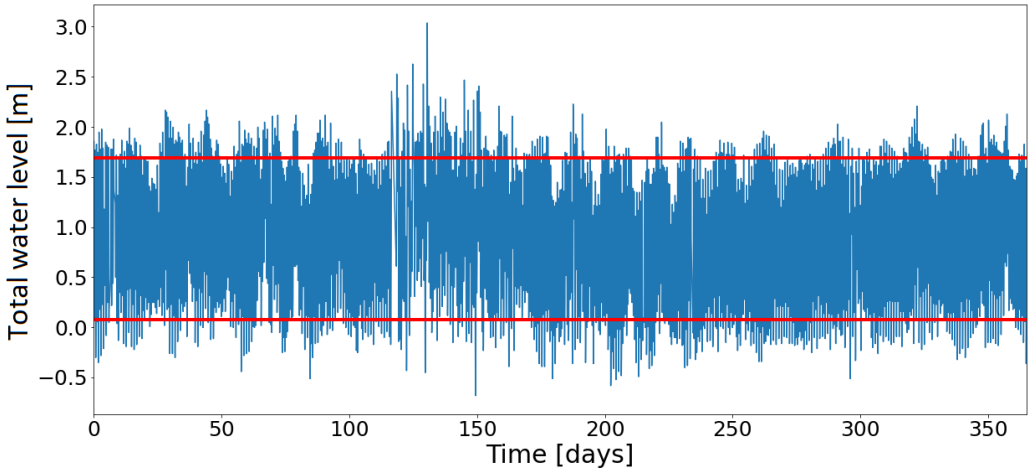

Figure 29 High and low water lines (red) plotted in total water level (still water level combined with runup, blue line), computed in Aeolis.

Based on these lines, intertidal and supratidal areas are determined. As explained in the limitations and assumptions section, the coastal profile changes too fast over time due to aeolian erosion and the lack of marine transport. Therefore, a time integrated cross-shore distance is calculated for both the intertidal as the supratidal area.

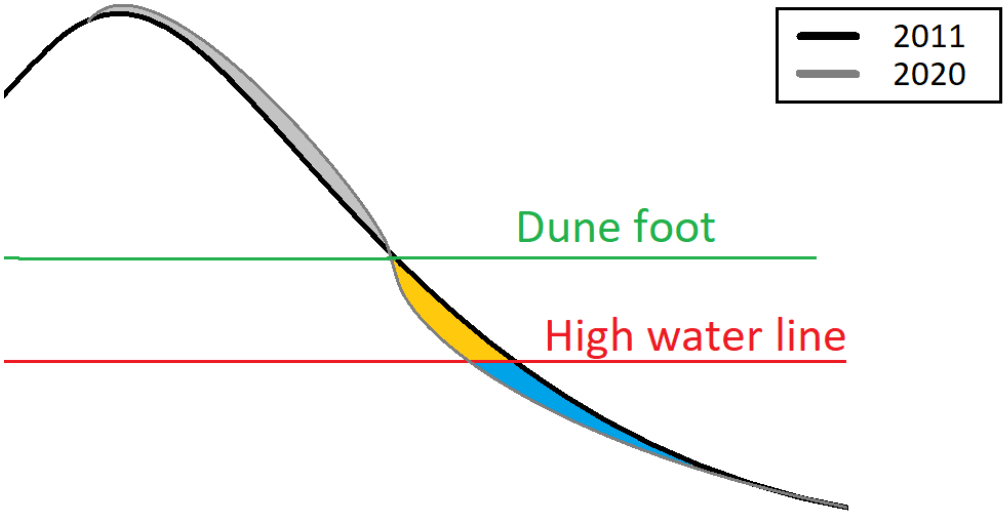

Figure 30 The change in cross-shore profile of the wide beach section over time, drawn schematically. The red line is the high-water line where the supratidal and intertidal area is split. The blue shaded area underneath the high-water line indicates the component of the intertidal area. The component of the supratidal area is indicated by the yellow shade.

For both areas, their contribution to the sediment flux towards the dunes is calculated. This is done by calculating the erosion per grid cell and determining if the cell is located in the intertidal or supratidal area. This process is repeated every modelled week to cope with the changing location of the shoreline (Fig 30).

Working hypothesis

It is expected that the change in sediment volume in the dunes is dependent on the beach width, as found by De Vriend & Roelvink [31]. The beach width in this study is defined as the distance between the dune foot and the low-water line. For the sake of comparison, the same definition is used in this raport. Oblique winds are therefore not accounted for in the beach width calculations.

Based on the working hypothesis, linear trends between MSWL and sediment flux are expected for the regular beach. At the Sand Motor, a different trend is expected since the coastal profile is non-linear. Consequent changes in ratio between intertidal and supratidal area could be of influence, according to B.M. Hoonhout and S. de Vries [38]. This study found that supratidal and intertidal zones have different effects on sediment supply.

6.2 Impact of increasing water levels at regular coasts

For the regular coast, the two sections as defined in section 6.1 will be analyzed. The beach boundaries in cross-shore direction are defined at the dune foot (3m NAP) and the mean low-water line, in line with the research of De Vriend & Roelvink [31]. For every scenario, a calculation of the beach width and cumulative sediment flux is made (Fig 31, green and red stars).

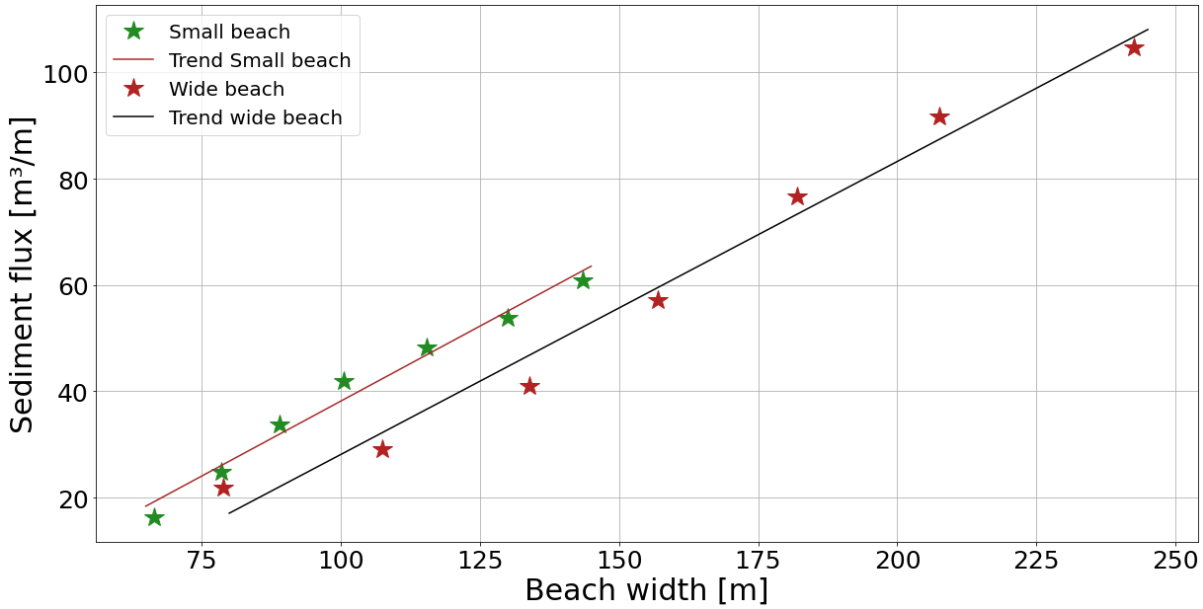

Figure 31 Sediment flux vs beach width. Outcomes of different water level scenarios are indicated with the stars. A trend line is plotted through the outcomes of all scenarios for both the small and wide beach sections.

Based on the working hypothesis, linear trends are expected for both the wide and small beach. The accuracy of these trends is quantified by the R^2 value, which is the coefficient of determination. For both the small beach and wide beach, a R^2 of 0.96 is found. Although the R^2 is close to 1 and the same for both sections, a somewhat hollow trend is seen for the wide beach section. The small beach section shows quite the opposite. To determine the underlying causes of this behavior, further analysis has been done. According to Hoonhout and De Vries [38] supratidal and intertidal zones have different effects on sediment supply. These different effects are analyzed according to the method described in the previous section.

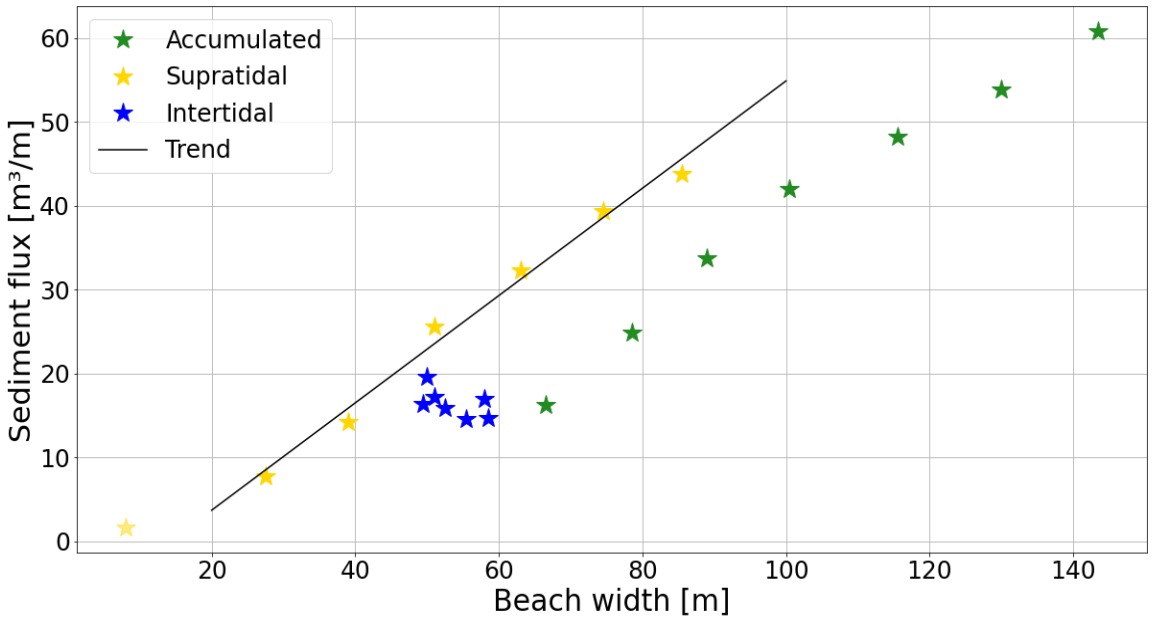

Figure 32 Small beach sediment flux vs width. The total sediment flux of different water level scenarios are indicated with green stars. This accumulated flux is split into supratidal and intertidal sediment flux, which are indicated with yellow and blue stars respectively. A trend line is plotted through the supratidal sediment fluxes of different scenarios.

For the small beach section, the outcome of the intertidal and supratidal differentiation in sediment supply is shown (Fig 32). The supratidal area (yellow) shows a linear relation between beach width and sediment flux between the scenarios. An exception is visible for the smallest supratidal width. This width is too small for an accurate calculation. For the intertidal area (blue) no trend is found.

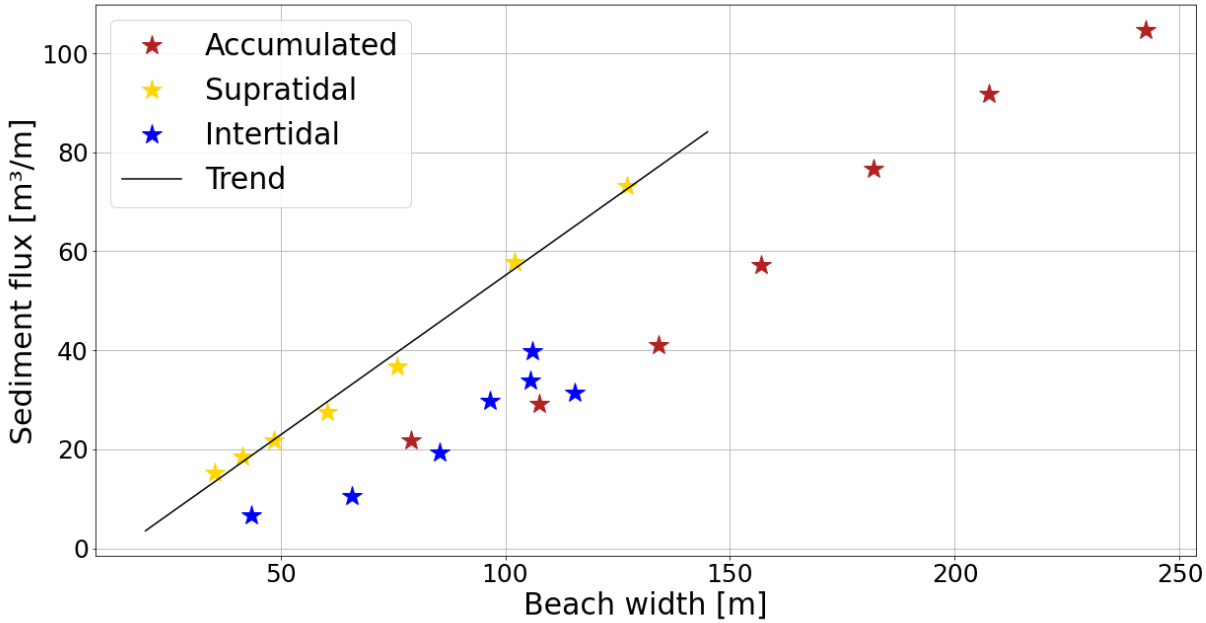

Figure 33 Wide beach' sediment flux vs width. The total sediment flux of different water level scenarios are indicated with red stars. This accumulated flux is split into supratidal and intertidal sediment flux, which are indicated with yellow and blue stars respectively. A trend line is plotted through the supratidal sediment fluxes of different scenarios.

The same results can be found for the wide beach section as for the small beach section. Again, a linear trend is found for the supratidal area, whereas the intertidal area trend is inconclusive (Fig 33).

Both figures are integrated (Fig 34). The supratidal relation between sediment flux and beach width, for both sections, follow the same linear trend. The sediment flux originating from the intertidal area is inconclusive. The accuracy of this trend, quantified by the R^2 value, is determined to be 0.99.

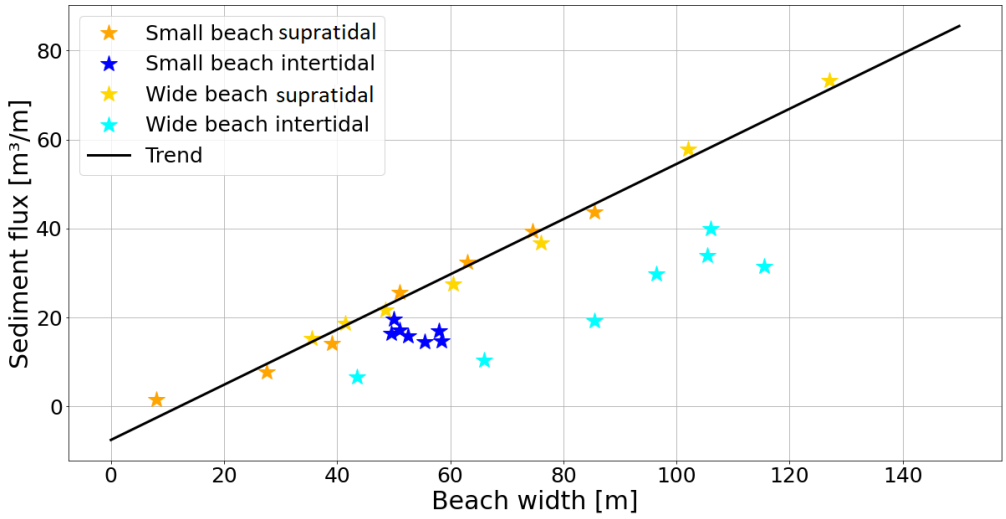

Figure 34 Supratidal trend, sediment flux vs beach width. Yellow and gold stars represent supratidal sediment flux for the supratidal area of the small and wide beach sections. Blue and lightblue stars represent sediment flux for the intertidal area of the small and wide beach sections. A trend line is plotted through the supratidal sediment flux outcomes.

For regular coasts, the relation stated in the working hypothesis specified in 2.3 can be improved, when only accounting for the supratidal area. The intertidal area should be left out since the sediment supply obscures the linear relation between beach width and sediment flux.

6.3 Impact of increasing water levels at the Sand Motor

For the Sand Motor domain, the same analysis is carried out. Notable differences between the regular coasts and the Sand Motor are a different type of coastal profile and the presence of extreme beach widths. To cope with these extreme widths, more SLR scenarios are simulated for more detailed insight. To check if the trend continues for extreme beach widths, an extra simulation is carried out where the supratidal beach width is greater than 800m. According to De Vries et al. [12], at large beach width, sediment flux towards the dunes is affected by the 'critical fetch effect'.

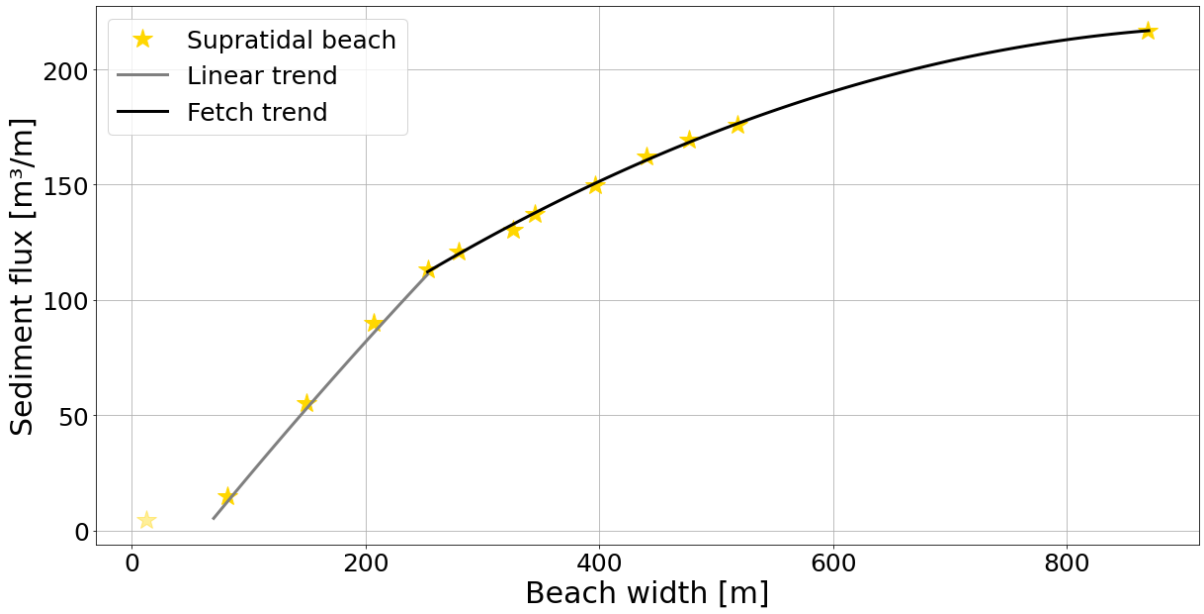

Figure 35 The sediment flux originating from the supratidal area vs the supratidal beach width, at the Sand motor section. The smallest beach width is too small to accurately determine the corresponding flux. Two different trendlines are plotted through the computed sediment fluxes.

The linear relation found for the regular coast is found for the Sand Motor coast as well (Fig 35). This holds for supratidal width from 80m up until around 250m, from which the critical fetch effect has an increasing influence on the sediment flux. This is in line with the findings of De Vries et al. [12]. For supratidal coasts wider than 250m, there is still a positive correlation between beach width and the sediment flux. This is due to two influences. First, Critical fetch length varies over time due to varying windspeed and direction. Second, armouring (supply limitation) prevents a completely saturated airflow. In this study, supratidal beach width is defined as the perpendicular length between the dune foot and the low-water line. Consequently, the named beach widths are not compensated for oblique wind directions. When compensating for the dominant wind direction, the beach widths and therewith the critical fetch length would increase.

6.4 Impact of modelled cross-shore profile change

The modelled aeolian sediment transport causes the cross-shore profile to change over time. With the dominant wind direction towards the dunes, sediment is eroded from the shoreline until the dune foot and is then deposited in the dunes, where vegetation increases the shear velocity threshold. The erosion is largest at the first dry cell past the shoreline, due to the largest gradient (section 2.2) and decreases towards the dune foot. Since there is no wave erosion module, nor marine transport module used in these simulations, there is no compensation for this duneward sediment transport. This results in a lowering of the cross-shore profile over time, with the largest

erosion around the shoreline and the least just in front of the dune foot, and accretion in the dunes (Fig 36).

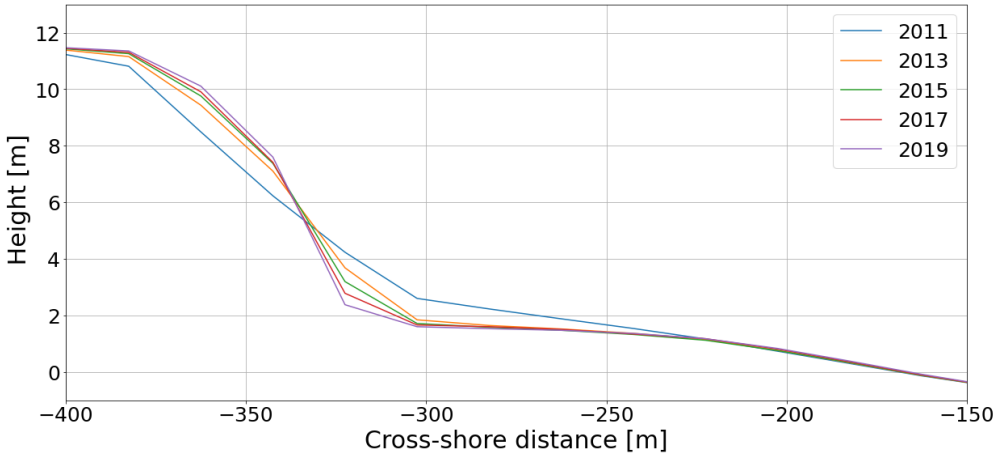

Figure 36 Computed cross-shore profile change between 2011 and 2019. Different colours represent the cross-shore profile of different years.

Although the modelled integrated dune growth and alongshore dune growth variation approximates the measured values (chapter 5), there is a difference in the predicted cross-shore profile change over time. In both situations, landward from the dune foot, dune growth is found. The modelled boundary between dunes and beach is very precise due to vegetation definition but in reality, this boundary is less distinctive. Furthermore, little change in cross-shore profile over time, between the shoreline and dune foot, is found (Fig 37). This is not reproduced by the model, where the beach profile is lowered over time.

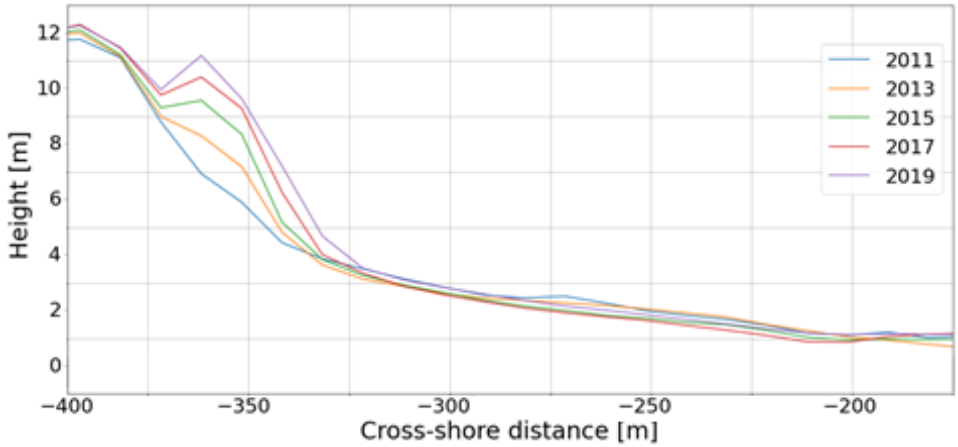

Figure 37 Measured cross-shore profile change between 2011 and 2019. Different colours represent the cross-shore profile of different years.

The absence of wave erosion at the dunes could be an explanation for the differences in cross-shore profile development. Modelled dune erosion caused by wave action could compensate the landward migration of sediment and restore the original profile. A second process that is neglected by the model is marine sediment supply in the intertidal area. Aeolian erosion in the profile could be compensated by subaqueous sediment transport.

7 Discussion, Conclusions and recommendations

7.1 Discussion

In this section, the results of this study are discussed. While the accuracy of the hindcasts are very promising, integrated sediment flux predicted 97% and 94% of the measured flux, several processes are currently not (fully) implemented. This impacts the interpretation of the model's results. For better understanding of the results, the influences of these processes are assessed.

Absence of marine transport

Measurements show large marine transport rates, especially during the first years after construction of the Sand Motor. One of the most important parameters used in this study is the beach width. Marine processes strongly impact the beach width and therewith the corresponding sediment flux towards the dunes. The absence of marine transport in this model causes discrepancies between measurements and simulations.
In a region which is as heavily impacted by marine transport as the Delfland domain, (after construction of the Sand Motor) it's impossible to accurately predict the dune development without incorporating these marine transports. This is confirmed by the high RMSE for the alongshore variation in dune growth found around the Sand Motor. At integrated level, these alongshore differences are levelled out, resulting in more accurate predictions.

Due to the large morphological changes at the Sand Motor and the adjacent coasts, only one year of the simulation (2013) could be used to assess the model's accuracy in terms of alongshore variation in the sediment flux towards the dunes.

The lack of wave erosion at the dune front in the model is another limitation coming forth out of the absence of marine transport. This holds that the volume of the simulated dunes can only increase over time. Where [31] found that 115m is the equilibrium beach width for regular beaches at the Holland coast, the model shows an increase in dune volume. Consequently, conclusions from beaches smaller than 115m should be taken cautiously.

As mentioned in chapter 3, the 'wet bed reset' process could be enabled to remain a steadier shoreline during the simulation. When disabled, the simulated shoreline retreat is too extreme, this results in a decreasing sediment availability. On the other hand, the wet bed reset process increases the amount of sediment in the domain, which is in contradiction with processes taking place in reality. However, as shown in appendix B, little differences in outcome were found between both methods.

Uniform grainsize distribution

It is currently impossible to simulate initial spatially varying bed compositions. As shown in chapter 5, the bed composition strongly influences the dune growth predictions. An initial 5% shelf content resulted in a total reduction sediment flux towards the dunes of 54%, or 62% after an amouring layer has been developed. This indicates the importance of correctly defining the sediment distributions. When the whole domain is simulated as nourished coast, the dune growth in the regular beach domain is lower than measured, because in reality no shelves are currently present at the regular beach. Due to (extreme) sea level rise, it's plausible that future coasts will consist of nourished sediment. The dune growth at the future coasts, could be more in line with the results of the simulations.

Model limitations

The model does not differentiate between the fluid and impact velocity threshold. The σ-value used in this model does not only represent the spatiotemporal averaged emergence of roughness elements but affects the fluid velocity threshold as well. Therefore, an unrealistically high σ-value is necessary to compensate for this. In the simulations, a shelves content of 5% reduces the sediment transport rate with 54%, which indicates the importance of this variable.
It's currently impossible to simulate rainfall. Rainfall has a sediment availability limiting effect. When the bed is moisty, sediment particles are more cohesive, resulting in an increased shear velocity threshold for aeolian transport. There is a correlation between storms and rainfall. During storms the transport capacity is largest. This induces great aeolian transport. Rainfall during storms would decrease the sediment availability and therewith the total simulated transport. Rainfall indirectly influences the armoured state of the coast as well. In case of less transport, the coast would take a longer time to reach an armoured state. This partly explains the discrepancy between measured and modelled dune growth in the initial stage of the simulations showed in chapter 5.

Results

A remarkable outcome of the simulations is the behavior of the intertidal area, in terms of sediment supply. No clear relation was found between the sediment supply and the length of the intertidal areas. This inconclusive behavior is hard to assess due to the absence of measured data. To improve understanding of these processes, more extensive study is necessary.
The critical fetch effects found in chapter 6 is based on beach width perpendicular to the coast. Since the dominant wind direction at the Delfland coast is west/ south-west, the effective fetch length is larger than the calculated 250m. The exact effective fetch length is hard to determine due to the temporal variation in wind direction and wind speed.

In contradiction with the findings of Hoonhout and de Vries [38], most of the sediment transported to the dunes originates from the supratidal area. This can be explained by the different definitions of supratidal area in this study compared with Hoonhout and de Vries [38]. The large contribution of the supratidal zone is due to the sporadically flooding of the lowest lying part. This induces mixing of the upper sediment layer whereafter an increased amount of sediment is again available for transportation. This combined with the almost permanently low moisture content results in the largest sediment supply of the domain. The bidaily flooding of the intertidal area, causes a transport-limitation due to moisture content. This has a larger negative effect on the total transported volume than the positive effect that comes with the bidaily mixing of the sediment. For optimal sediment supply, low-lying supratidal area should be maximized.

However, evaluation of the cross-shore profile development shows differences between the simulations and measurements. This could be an indication that not all processes are captured well or are still missing in the model. The lack of marine transport is likely to be a large factor in this dissimilarity between model and measurements but other influences cannot be ruled out. A coupled hydrodynamic-aeolian model could resolve this problem. Otherwise more research is needed to correctly implement the governing processes.

Generalization case study

Since the model is only validated for this specific case study, the question rises if the model is applicable in different situations. First, all natural processes are generally described such that the model can be applied at various locations. Input parameters specify the locally specific conditions present. While no extra calibration is performed for the regular coast, the dune growth is simulated with comparable accuracy as for the Sand Motor. However, the location of the regular beach is

similar to the location of the Sand Motor. Consequently, it remains unknown if the model is still applicable when simulating for instance another climate zones, where possibly not all processes are yet identified.

7.2 Conclusion

There are many processes affecting dune growth at the Delfland coast, with several processes even not yet identified. Wind forcing plays a crucial role in mobilization and transportation of sediment towards the dunes. This transportation volume is limited by the sediment availability, which is on its turn dependent on local influences such as moisture, vegetation and armouring processes. Consequently, dune growth shows to be a dynamic process in both space and time. Previously found dune growth relations turned out to be not capable of correctly predicting such a dynamic process but the process-based model AeoLis showed very promising simulation results. Dune growth simulations at the Delfland dunes between 2011 and 2020, compared with measured data proved to be a significant step forward in the understanding and describing of the processes present in at the coast.

The computed averaged dune growth in the Sand Motor domain during the first 3 years after construction is 39.5 m^3/m, where the measurements show a dune growth of 40.6 m^3/m. At the regular beach the averaged computed dune growth was 50.8 m^3/m. The measurements at this location showed a dune growth of 50.4 m^3/m. Both the Sand Motor and regular beach predictions proved to be very accurate. However, the final year of the simulation showed larger deviations from the measured values. This is explained by the absence of marine sediment transport in the model, as described in the discussion. A standalone aeolian process-based model is not capable to make long term simulations at locations where large morphological changes take place during the simulated period. For this, a hydrodynamic-aeolian coupled simulation could be the solution to keep up with the morphological change and corresponding changes in sediment availability.

Another promising result was simulation of the alongshore variation in dune growth. Despite the differences between model and reality, such as the presence of beach clubs and walkways in reality and the shadow effect due to dune vegetation definition in the model, the variation in alongshore dune growth is captured well. At the Sand Motor, during both the second and third year, when armouring in both the model and reality took place, the computed variability was within 10% of the measured value.

It is currently impossible to simulate spatial non-uniform grainsize distributions. When simulating a spatial uniform grainsize distribution including 5% non-erodible particles that are present in the Sand Motor nourishment, there is a reduction of the sediment flux of 54% compared with the situation without non-erodible particles. This shows the importance of being able to correctly define grainsize distributions. For simulations of domains with varying bed composition, it's crucial to implement spatially non-uniform grainsize distributions.

Water level change impacts the beach width, dependent on the coastal profile, on which the sensitivity for water level change is determined. A reduced beach width limits the sediment availability and the subsequent transport. Previous studies [31] linked the dune growth to the total beach width but in this research, it is found that supply of the intertidal area obscures this relation. The relation between the supratidal beach width and sediment flux towards the dunes holds for both a regular coastal profile and the profile of the Sand Motor. However, deviations in cross-shore development between measurements and computations show that not all processes are currently captured by the model. This is an indication that further research is required to improve the model. A critical fetch effect as predicted by De Vries et al. [12] is found for supratidal beach widths greater than 250m. For supratidal beaches greater than 250m, despite the fetch effect, there is still a positive correlation between beach width and the sediment flux. This is due to armouring processes and variable wind direction and speed.

7.3 Recommendations

During this study, several interesting points of improvement of the model came to light.

Coupled model

Although the integrated dune growth predictions of 2013 are very accurate, 94% in the Regular beach domain and 97% in the Sand Motor domain, the prediction of the ultimate dune growth is significantly less accurate. This is largely explained by the lack of marine morphological development. The most prominent improvement for this model would be to couple it with a model that simulates subaqueous sediment transport. This way the morphological change due to marine processes is incorporated into the model. In case of the Sand Motor, this would mean that the deformation of the peninsula and the spreading of its sediment towards the adjacent coasts would be captured. Corresponding changes in beach width and sediment availability would greatly improve the long-term predictions of dune growth in the Delfland domain. The subaqueous model should be able to simulate wave erosion on the dune front in case of extreme storms as well. This holds that the cross-shore sediment cycle as mentioned in [31] can be simulated.

Multiple grainsize distributions

This study focused on the dune development in the lee of nourished coasts. Other studies may be interested in domains where both a nourished coast and a regular coast are present. The sediment used for the Sand Motor nourishment consisted for 5% of shelves. This initial 5% shelf content resulted in a total reduction sediment flux towards the dunes of 54%. This is an indication for the importance of being able to define the correct sediment distributions. Ideally no compromise should be made when different initial grainsize distributions are present in a domain.

Implementing rainfall module

As previously mentioned, rainfall often occurs during storm events. The extreme high wind speeds increase the aeolian transport significantly. In reality, this aeolian transport during storms is limited by increased soil moisture content due to rainfall. The model currently does only consider the increased wind speeds, which results in an overestimation of aeolian sediment transport during storms. Since the aeolian transport capacity exponentially grows with an increasing wind speed and rainfall is likely to be present at storms (extreme wind speeds), this overestimation could be substantial. Next to its immediate influence on the transport rate, armouring processes would be slowed down as well. This would presumably result in a better prediction of the dune growth during the first year of a simulation.

Timescale expansion

In this study, aeolian transports are simulated for the duration of 10 years. On a 10-year timescale, yearly increasing MSWL has very limited effects of the dune growth. Therefore, only an initial instantaneous increase of the MSWL is used in this study. Ideally the simulation timescale should be increased to about 20-30 years to be able to assess the impact of the temporal increasing MSWL. Due to the lack of subaqueous sediment transport, the gap between the simulated bathymetry and reality becomes substantially larger every year. Consequently, comparing the model's results with the measured data becomes increasingly challenging. In case of the Delfland, Sand Motor domain, the accuracy of the alongshore variation in dune growth could only be assessed during the 1.5 years. The timescale expansion could possibly be achieved by using a coupled model such as described earlier in this section.

Cross-shore behavior

More research should be done about the cross-shore profile change of a coast. Current processes that are implemented in the model logically result in lowering of the beach over time. In reality, this behavior is not found. Subaqueous supply of sediment, as well as wave erosion at the dunes could be of importance to resolve this discrepancy.

Literature

[1] Hoonhout, B., De Vries, S. (2018) *Simulating Spatiotemporal Aeolian Sediment Supply at a Mega Nourishment.* Technical University Delft, 2018

[2] Kustonderhoud Rijkswaterstaat https://www.rijkswaterstaat.nl/water/waterbeheer/bescherming-tegen-het-water/maatregelen-om-overstromingen-te-voorkomen/kustonderhoud. Consulted 31-01-2022

[3] Van Koningsveld, M., & Mulder, J. P. M. P. M. (2004). *Sustainable coastal policy developments in the Netherlands. A systematic approach revealed.* Journal of coastal research 20(2), 375-385, 2005

[4] ROELSE, P., 2002. *Water en Zand in Balans. Evaluatie zandsuppleties na 1990; een morfologische beschouwing.* Report RIKZ-2002.003. ISBN 90-36-369-3426-5. (In Dutch)

[5] Nicholls, R.J. & Cazenave, A. (2010) *Sea-Level Rise and Its Impact on Coastal Zones.* Science, 2010.

[6] IPCC 2021, *Climate Change 2021 The Physical Science Basis.* Working Group I Technical Support Unit, 2021.

[7] Klimaatsignaal'21 *Hoe het klimaat in Nederland snel verandert.* KMNI,2021.

[8] Ranasinghe, R. (2016). Assessing climate change impacts on open sandy coasts: A review Earth Science Reviews. p.321.

[9] Nicholls, R.J., P.P. Wong, V.R. Burkett, J.O. Codignotto, J.E. Hay, R.F. McLean, S. Ragoonaden and C.D. Woodroffe, (2007): *Coastal systems and low-lying areas. Climate Change 2007: Impacts, Adaptation and Vulnerability.* Contribution of Working Group II to the Fourth Assessment Report of the Intergovernmental Panel on Climate Change, M.L. Parry, O.F. Canziani, J.P. Palutikof, P.J. van der Linden and C.E. Hanson, Eds., Cambridge University Press, Cambridge, UK, 315-356.

[10] Bruun, P. (1988) *The Bruun Rule of Erosion by Sea-Level Rise: A Discussion on Large-Scale Two- and Three- Dimensional Usages*. Coastal Education & Research Foundation, 1988.

[11] Scientific Committee on Ocean Research (SCOR) (1991). *The Response of Beaches to Sea-Level Changes: A Review of Predictive Models.* Coastal Education & Research Foundation, 1991.

[12] De Vries, S., Arens B., Stive, M., Ranasginghe, R. (2011). *Dune growth trends and the effect of beach width on annual timescales.* Geomorphology, 2018.

[13] Cooper, J. A. G. and Pilkey, O. H. (2004). *Sea-level rise and shoreline retreat: Time to abandon the Bruun Rule.* Global and Planetary Change, 43(3), p. 157-171.

[14] Ranasinghe, R. and Stive, M. J. F. (2009*). Rising seas and retreating coastlines*. Climatic Change 97**,** p. 465.

[15] Van Rijn, L. C. (1997). *Sediment transport and budget of the central coastal zone of Holland*. Coastal Engineering 32.1, pp. 61–90.

[16] Hoonhout, B.M. (2017). Aeolian sediment availability and transport. PhD thesis, Technical University Delft, 2017.

[17] Rijkswaterstaat (2011). *Kwaliteitsdocument laseraltimetrie deel 1 & deel 2, perceel 1 & 2*

[18]: van Houdt, J., Linnartz, L., ARK Natuurontwikkeling (2012*). Eén jaar Zandmotor Natuurontwikkelingen op een dynamisch stukje Nederland.* ARK Natuurontwikkeling, 2012.

[19] De Zeeuw, R.C. (2012). *Veldrapportage #1.* NeMo, 2012.

[20] McKenna Neuman, C., Li, B., and Nash, D. (2012). *Micro573 topographic analysis of shell pavements formed by aeolian transport in 574 a wind tunnel simulation*. Journal of Geophysical Research, 117(F4). 575 doi:10.1029/2012JF002381. F04003.

[21] Ministerie van Verkeer en Waterstaat. (2010*) Projectnota/MER: Aanleg en zandwinning Zandmotor Delflandse kust*. Projectnota MER, 2010.

[22] Google Earth images https://earth.google.com. Retrieved 03-02-2022 & 20-02-2023.

[23] Bagnold, R.A. (1937). *The Transport of Sand by Wind.* The Geographical Journal, 1937.

[24] Hoonhout, B.M. (2018) *AeoLiS Documentation*. https://aeolis.readthedocs.io .

[25] Martínez, M.L., Intralawan, A., Vázquez, G., Pérez-Maqueo, O., Sutton, P., Landgrave, R. (2007). *The coasts of our world: Ecological, economic and social importance.* Ecological Economics, 2007.

[26] Luijendijk, A.P., van Oudenhoven, A. (2019). *The Sand Motor: A Nature-Based Response to Climate Change Findings and Reflections of the Interdisciplinary Research Program NatureCoast*. Delft University Publishers, 2019.

[27] Neumann, B., Athanasios, Vafeidis, T., Zimmermann, J., Nicholls, R.J., 2015. *Future Coastal Population Growth and Exposure to Sea-Level Rise and Coastal Flooding - A Global Assessment.* PLoS ONE 10, 2015.

[28] Velhorst, R.C.L. (2017). *Towards a coupled morphodynamic model of the nearshore zone and the beach at the sand engine*. Delft University of Technology,May 2017.

[29] Davidson-Arnott, R.G.D., Law, M.N. (1996). *Measurement and prediction of long-term sediment supply to coastal foredunes.* Journal of coastal research 12, 1996.

[30] de Schipper, M.A., de Vries, S., Ruessink, G., de Zeeuw, R.C., Rutten, J., van Gelder-Maas, C., and Stive, M.J.F. (2016*). Initial spreading of a mega feeder nourishment: Observations of the Sand Engine pilot project. Coastal Engineering*, www.elsevier.com/locate/coastaleng, 2016.

[31] de Vriend, H.J. and Roelvink, J.A. (1989*). Innovatie van kustverdediging: inspelen op het kustsysteem. Kustverdediging na 1990, technisch rapport 19*. Technical report, Delft Hydraulics rapport H825, 1989.

[32] Nicholls, R., Brown, S., Hanson, S. (2010). *Economics of Coastal Zone Adaptation to Climate Change.* The world bank paper 10., 2010.

[33] Ministerie van Infrastructuur en Milieu, Rijkswaterstaat (2015). *Ons Water in Nederland.* Ministerie van Infrastructuur en Milieu, 2015.

[34] van Duin, M.J.P., Wiersma, N.R., Walstra, D.J.R., van Rijn, L.C. (2004). *Nourishing the shoreface: observations andasting of the Egmond case, The Netherlands.* Coastal Engineering 51, 2004
[35] Brand, E., Ramaekers, G., Lodder, Q. (2022). *Dutch experience with sand nourishments for dynamic coastline conservation – An operational overview.* Ocean and Coastal Management, 2022.

[36] Pilarczyk, K.W., Verhagen, H.J., Roelse, P., Adriaanse, L., Consemulder, J. (1988). *Handboek Zandsuppleties.* Rijkswaterstaat, 1988.

[37] Van der Spek, A.J.F., de Kruif, A.C., Spanhoff, R. (2007). *Richtlijnen Onderwatersuppleties.* Technical University Delft, 2007

[38] Hoonhout, B.M., de Vries, S. (2017) *Aeolian Sediment Supply at a Mega Nourishment.* Technical University Delft, 2017

[39] Kust-viewer https://www.openearth.nl/coastviewer-static/ retrieved 05-08-2022

[40] Leenders J.K., Van Boxel J.H., Sterk G. (2007). The effect of single vegetation elements on wind speed and sediment transport in the Sahelian zone of Burkina Faso. Earth Surface Processes and Landforms 2005.

[41] Greeley R., Iversen J.D. (1985). Wind as a Geomorphological Process. Cambridge Planetary Science Series, 1985.

Appendix

A Parameters, masks and forcing

Here a complete list of parameter settings, used for the reference simulation is given. Below the parameter list, the used masks are displayed. The last section of this appendix shows the forcing timeseries.

[Timing]			
dt		3600	% [s] Timeinterval between timesteps
[Flags Processes]			
process_wind	T		% [T/F] Enable the process of wind
process_shear	T		% [T/F] Enable the process of wind shear
process_tide	T		% [T/F] Enable the process of tides
process_wave	T		% [T/F] Enable the process of waves
process_runup	T		% [T/F] Enable the process of wave runup
process_moist	T		% [T/F] Enable the process of moist
process_mixtoplayer	T		% [T/F] Enable the process of mixing
process_threshold	T		% [T/F] Enable the process of threshold
process_transport	T		% [T/F] Enable the process of transport
process_bedupdate	T		% [T/F] Enable the process of bed updating
process_salt	F		% [T/F] Enable the process of salt
process_humidity	F		% [T/F] Enable the process of humidity
process_avalanche	T		% [T/F] Enable the process of avalanching
process_separation	F		% [T/F] Enable the including of separation bubble
process_vegetation	T		% [T/F] Enable the process of vegetation
process_fences	F		% [T/F] Enable the process of sand fencing
[Flags Threshold]			
th_grainsize	T		% [T/F] Enable wind velocity threshold based on grainsize
th_moisture	T		% [T/F] Enable wind velocity threshold based on moisture
th_drylayer	F		% [T/F] Enable wind velocity threshold based on drying of layer
th_sheltering	T		% [T/F] Enable wind velocity threshold based on roughness
th_nelayer	F		% [T/F] Enable wind velocity threshold based on a non-erodible layer
[General physics]			
g		9.81	% [m/s^2] Gravitational constant
v		0.000015	% [m^2/s] Air viscosity
rhoa		1.225	% [kg/m^3] Air density
rhog		2650	% [kg/m^3] Grain density
rhow		1025	% [kg/m^3] Water density
porosity		0.4	% [-] Sediment porosity
cpair		0.001004	% [m] Average grain size of each sediment fraction

[Sediment]		
nlayers	10	% [-] Number of bed layers
layer_thickness	0.01	% [m] Thickness of bed layers
nfractions	11	% [-] Number of sediment fractions
grain_dist	0.005709 0.234708 0.608887 0.099666 0.001029 0.000001 0.010486 0.028503 0.010486 0.000522 0.000004	% [-] Initial distribution of sediment fractions
grain_size	0.000177 0.000250 0.000354 0.000500 0.000707 0.001000 0.002000 0.004000 0.008000 0.016000 0.032000	% [m] Average grain size of each sediment fraction
[Wind and shear]		
wind_convention	nautical	% [-] Convention used for the wind direction in the input files (cartesian or nautical)
alfa	0	% [deg] Real-world grid cell orientation wrt the North (clockwise)
k	0.01	% [m] Bed roughness
z	10	% [m] Measurement height of wind velocity
kappa	0.41	% [-] Von Kármán constant
h	None	% [m] Representative height of saltation layer
L	100	% [m] Typical length scale of dune feature (perturbation)
l	1	% [m] Inner layer height (perturbation)
m	0.5	% [-] Factor to account for difference between average and maximum shear stress
[Transport]		
bi	0.05	% [-] Bed interaction factor
method_transport	bagnold	% [-] Name of method to compute equilibrium sediment transport rate
method_grainspeed	windspeed	% [-] Name of method to assume/compute grainspeed
Aa	0.085	% [-] Constant in formulation for wind velocity threshold based on grain size
Cb	1.5	% [-] Constant in bagnold formulation for equilibrium sediment concentration
Ck	2.78	% [-] Constant in kawamura formulation for equilibrium sediment concentration
Cl	6.7	% [-] Constant in lettau formulation for equilibrium sediment concentration
Cdk	5	% [-] Constant in DK formulation for equilibrium sediment concentration
[Solver]		
T	1	% [s] Adaptation time scale in advection equation
solver	pieter	% [-] Numerical solver of advection scheme
CFL	1	% [-] CFL number to determine time step in explicit scheme
accfac	1	% [-] Numerical acceleration factor
scheme	euler_backward	% [-] Name of numerical scheme (euler_forward, euler_backward or crank_nicolson)

max_error		0.00001
max_iter		1000
max_bedlevel_change		0.01
[Boundary conditions]		
boundary_onshore	constant	
boundary_lateral	circular	
boundary_offshore	constant	
offshore_flux		0
constant_offshore_flux		0
onshore_flux		0
constant_onshore_flux		0
lateral_flux		0
sedimentinput		0
[Vegetation]		
sigma		11.9
beta		130
gamma_vegshear		50
avg_time		86400
dzb_interval		86400
hveg_max		1
dzb_opt		0
V_ver		50
V_lat		0
germinate		0
lateral		0
veg_gamma		1
veg_sigma		0.8
vegshear_type	raupach	

% [-] Maximum error at which to quit iterative solution in implicit numerical schemes
% [-] Maximum number of iterations at which to quit iterative solution in implicit numerical schemes
% [m] Maximum bedlevel change after one timestep. Next timestep dt will be modified (use 999. if not used)

% [-] Name of onshore boundary conditions (flux, constant, uniform, gradient)
% [-] Name of lateral boundary conditions (circular, constant ==noflux)
% [-] Name of offshore boundary conditions (flux, constant, uniform, gradient)
% [-] Factor to determine offshore boundary flux as a function of Q0 (= 1 for saturated flux , = 0 for noflux)
% [kg/m/s] Constant input flux at offshore boundary
% [-] Factor to determine onshore boundary flux as a function of Q0 (= 1 for saturated flux , = 0 for noflux)
% [kg/m/s] Constant input flux at offshore boundary
% [-] Factor to determine lateral boundary flux as a function of Q0 (= 1 for saturated flux , = 0 for noflux)
% [-] Constant boundary sediment influx (only used in solve_pieter)

% [-] Ratio between basal area and frontal area of roughness elements
% [-] Ratio between drag coefficient of roughness elements and bare surface
% [-] Roughness factor for the shear stress reduction by vegetation
% [s] Indication of the time period over which the bed level change is averaged for vegetation growth
% [s] Interval used for calcuation of vegetation growth
% [m] Max height of vegetation
% [m/year] Sediment burial for optimal growth
% [m/year] Vertical growth
% [m/year] Lateral growth
% [1/year] Possibility of germination per year
% [1/year] Posibility of lateral expension per year
% [-] Constant on influence of sediment burial
% [-] Sigma in gaussian distrubtion of vegetation cover filter
% [-] Choose the Raupach grid based solver (1D or 2D) or the Okin approach (1D only)

okin_c1_veg		0.48	% [-] x/h spatial reduction factor in Okin model for use with vegetation
okin_initialred_veg		0.32	% [-] initial shear reduction factor in Okin model for use with vegetation
[Soil moisture]			
Tdry		5400	% [s] Adaptation time scale for soil drying
eps		0.001	% [m] Minimum water depth to consider a cell "flooded"
method_moist	belly_johnson		% [-] Name of method to compute wind velocity threshold based on soil moisture content
[Avalanching]			
theta_dyn		33	% [degrees] Initial Dynamic angle of repose, critical dynamic slope for avalanching
theta_stat		34	% [degrees] Initial Static angle of repose, critical static slope for avalanching

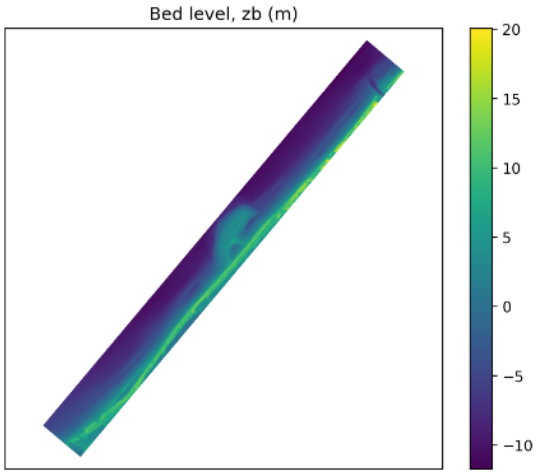
Bed level, zb (m)
20
15
10
5
0
−5
−10

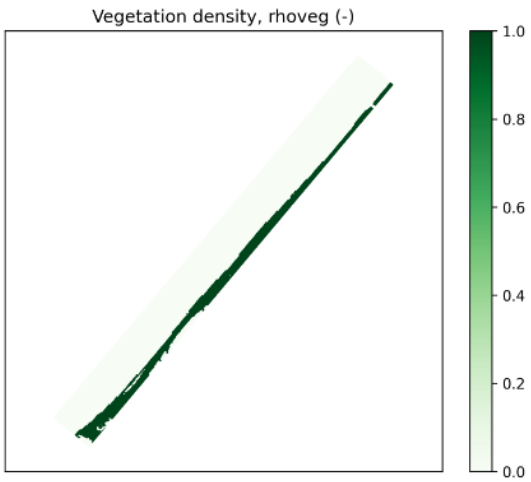
Vegetation density, rhoveg (-)
1.0
0.8
0.6
0.4
0.2
0.0

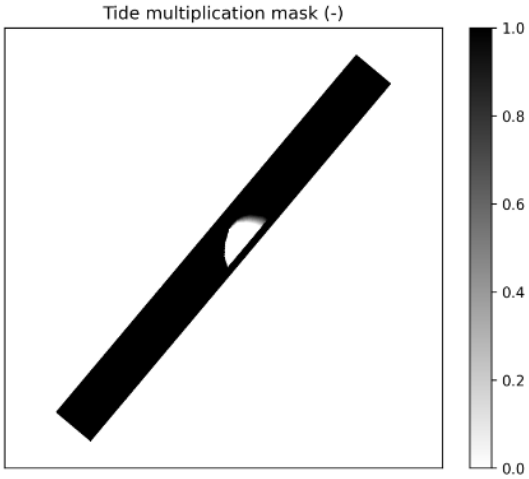
Tide multiplication mask (-)
1.0
0.8
0.6
0.4
0.2
0.0

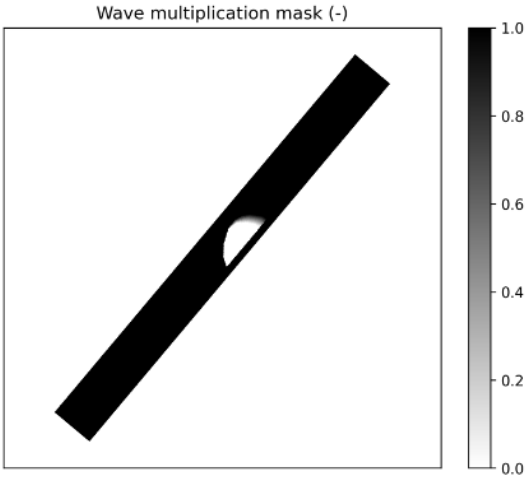
Wave multiplication mask (-)
1.0
0.8
0.6
0.4
0.2
0.0

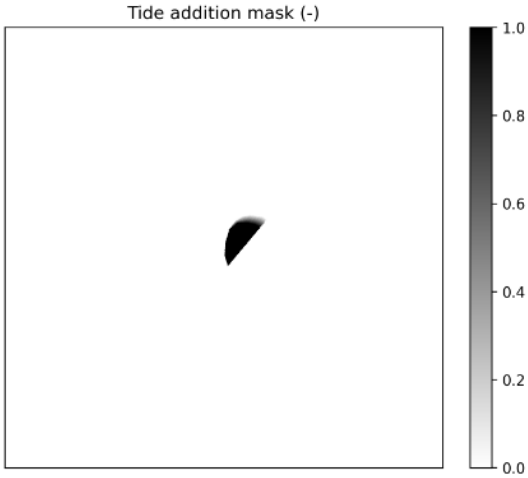
Tide addition mask (-)
1.0
0.8
0.6
0.4
0.2
0.0

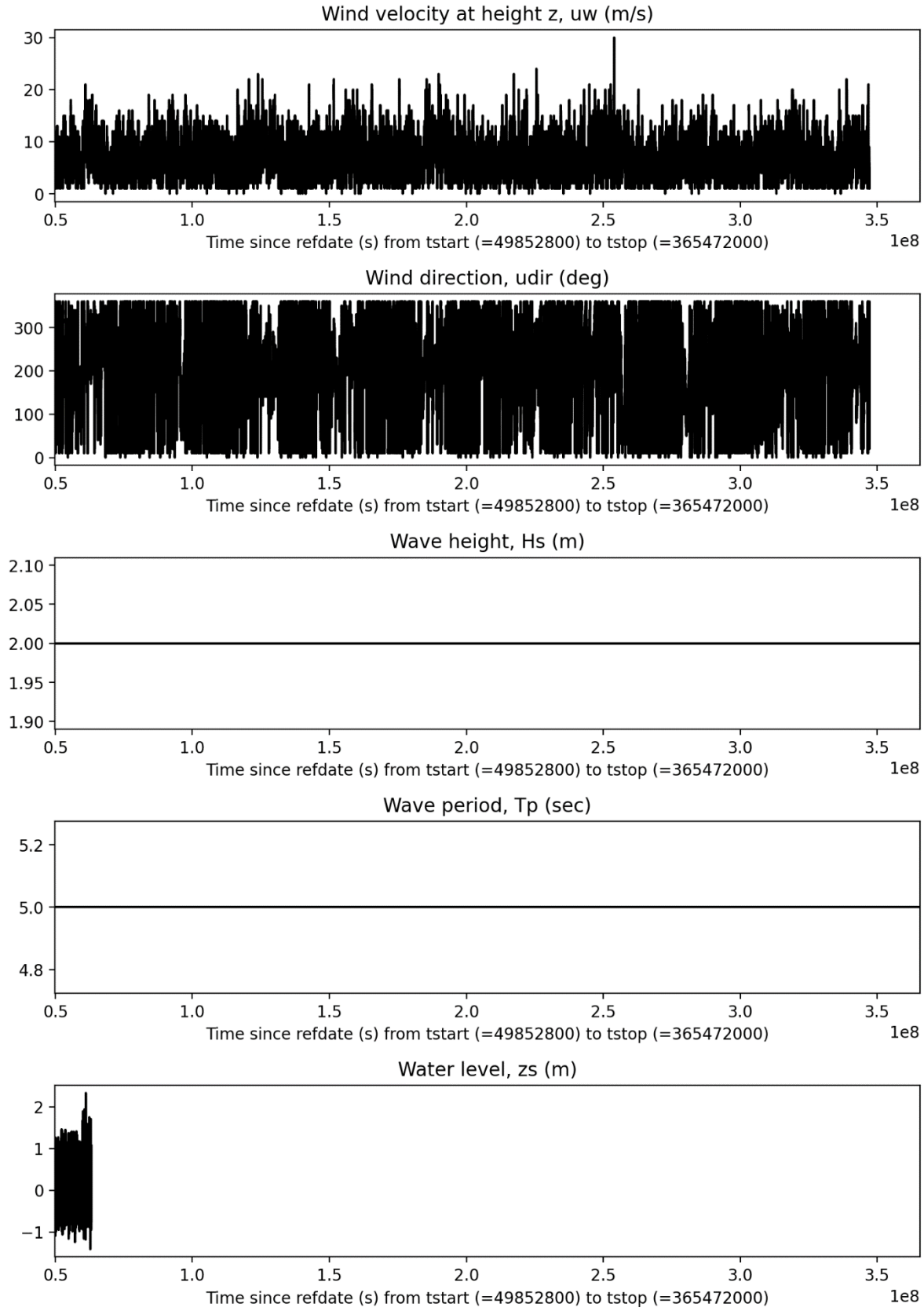
Wind velocity at height z, uw (m/s)
30
20
10
0
0.5
1.0
1.5
2.0
2.5
3.0
3.5
Time since refdate (s) from tstart (=49852800) to tstop (=365472000)
1e8
Wind direction, udir (deg)
300
200
100
0
0.5
1.0
1.5
2.0
2.5
3.0
3.5
Time since refdate (s) from tstart (=49852800) to tstop (=365472000)
1e8
Wave height, Hs (m)
2.10
2.05
2.00
1.95
1.90
0.5
1.0
1.5
2.0
2.5
3.0
3.5
Time since refdate (s) from tstart (=49852800) to tstop (=365472000)
1e8
Wave period, Tp (sec)
5.2
5.0
4.8
0.5
1.0
1.5
2.0
2.5
3.0
3.5
Time since refdate (s) from tstart (=49852800) to tstop (=365472000)
1e8
Water level, zs (m)
2
1
0
−1
0.5
1.0
1.5
2.0
2.5
3.0
3.5
Time since refdate (s) from tstart (=49852800) to tstop (=365472000)
1e8

B Simulation choices

Three choices made in chapter 3 will be elaborated on in this appendix. First the option ‘wet bed reset’ will be discussed. Then, the choice for the increased water (or soil moisture) level in the lake and lagoon is explained.

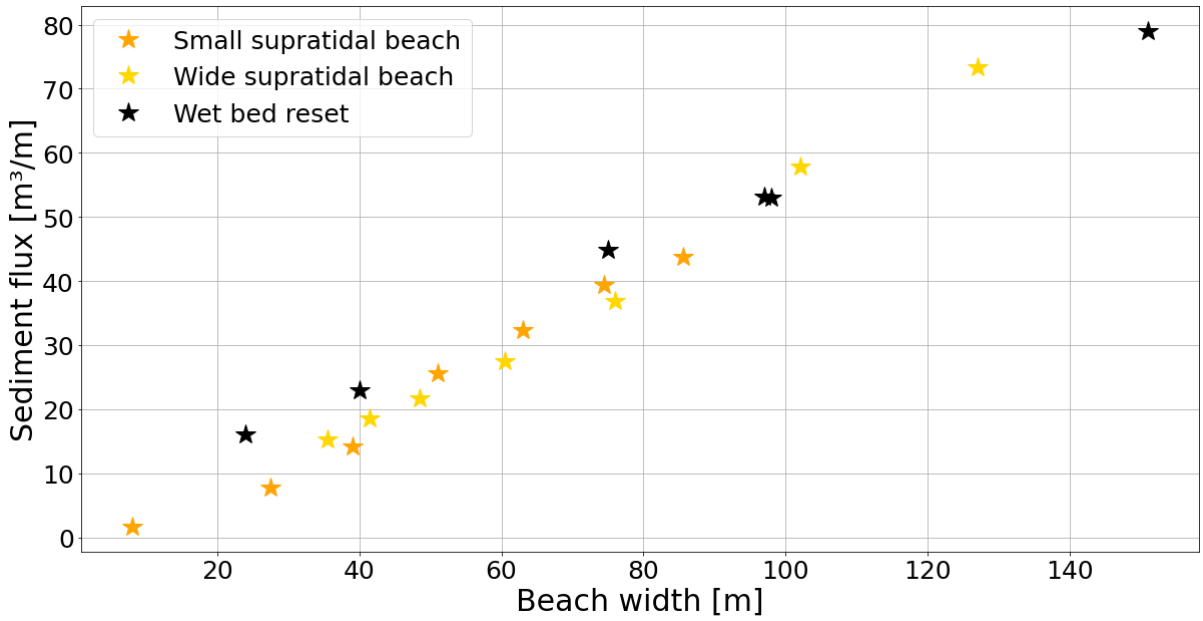

Figure 38 Wet bed reset enabled vs disabled

The gold and yellow stars (Fig 38) show the sediment flux corresponding to the supratidal beach widths for simulations with the ‘wet bed reset’ process disabled. The black stars stand for the simulations with the process enabled. For both scenarios, a linear trend can be seen although there is a small deviation in slope of these trends. This can be explained by the addition of sediment into the domain in the simulations with ‘wet bed reset’ enabled. This induces an increased amount of dry, for sediment transportation susceptible, area in the intertidal zone, which results in a larger amount of mobilized sediment. Therefore, the gradient at the supratidal beach is lowered as is the supply of the supratidal area.

The cross-shore LIDAR plot at the lake section (Fig 39), shows that over time the lake fills up with sediment. Note that LIDAR campaign can only measure until a limited depth, meaning that the original lake is in reality deeper than shown in the plot.

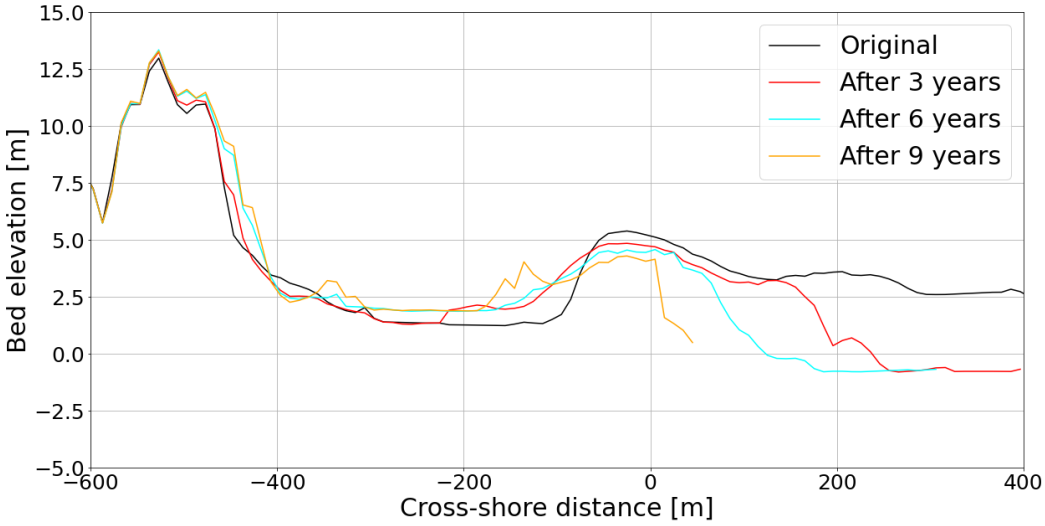

Figure 39 Cross-shore plot of the lake section

The bed level at the lake stabilizes at a height of 2m (Fig 39). This holds that sediment accreting at the lake higher in the profile than at 2m NAP is susceptible for transportation while sediment lower than the 2m threshold is not. For more accurate predictions of the alongshore variation in dune growth at the Sand Motor, the still water level in the lake and lagoon is increased to 2m.

C Alongshore dune growth

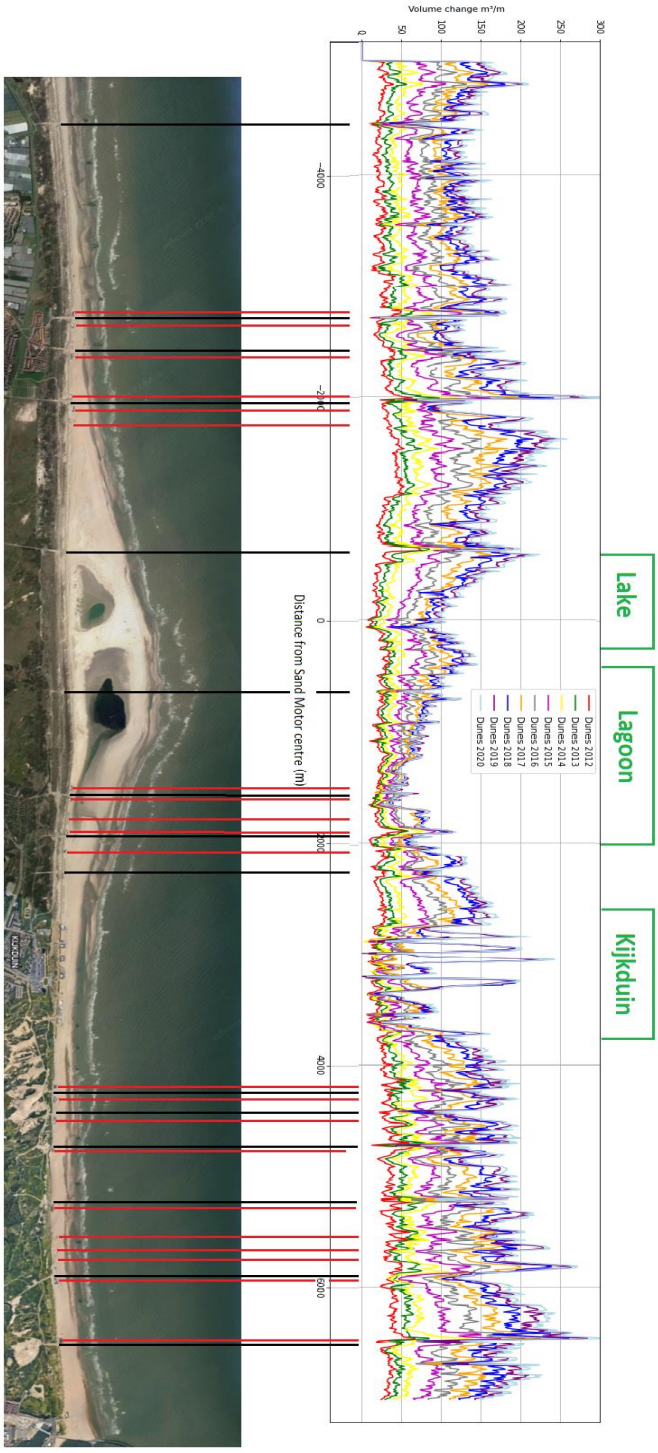

Figure 40 Depressions in alongshore dune growth (upper plot) and their location (lower plot). Red lines indicate beach clubs' location, black lines indicate walkways.

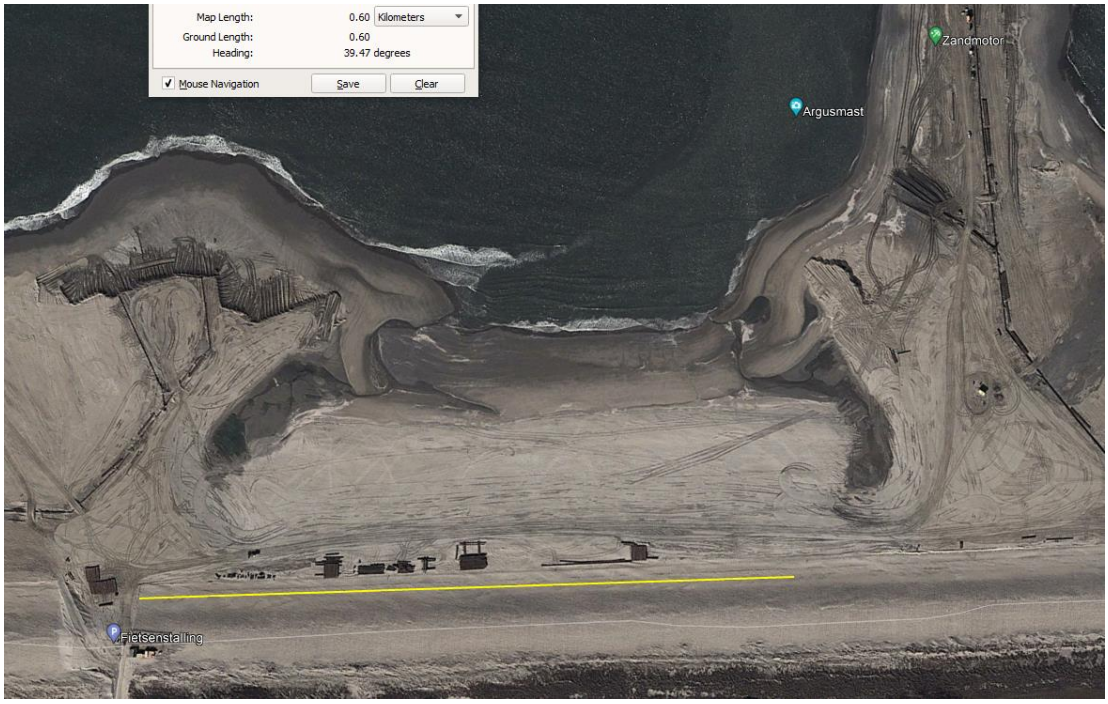

Figure 41 Human interference in the dune system at x = -600m; 'Fietsenstalling' [22].

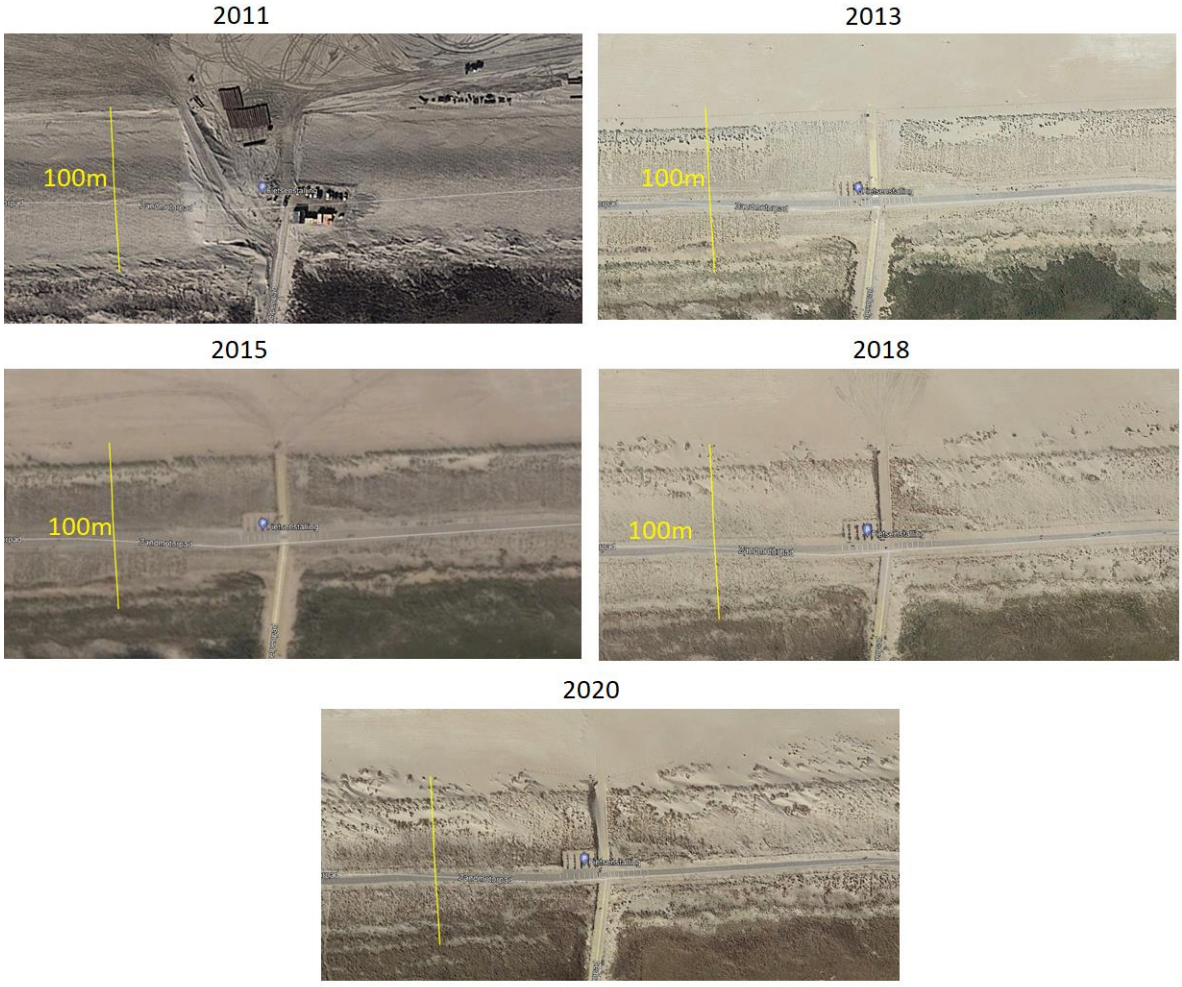

Figure 42 Evolution of the dunes around the 'Fietsenstalling' from 2011 until 2020.